BRNO UNIVERSITY OF TECHNOLOGY
VYSOKÉ UČENÍ TECHNICKÉ V BRNĚ

FACULTY OF MECHANICAL ENGINEERING
FAKULTA STROJNÍHO INŽENÝRSTVÍ

INSTITUTE OF MATHEMATICS
ÚSTAV MATEMATIKY

MATHEMATICAL MODELLING OF WALKING ROBOTS
MATEMATICKÉ MODELOVÁNÍ KRÁČEJÍCÍCH ROBOTŮ

MASTER'S THESIS
DIPLOMOVÁ PRÁCE

AUTHOR
AUTOR PRÁCE

Bc. Daniel Kiša

SUPERVISOR
VEDOUCÍ PRÁCE

doc. Ing. Petr Tomášek, Ph.D.

BRNO 2020

BRNO UNIVERSITY OF TECHNOLOGY
FACULTY OF MECHANICAL ENGINEERING

Specification Master's Thesis

Department:	Institute of Mathematics
Student:	**Bc. Daniel Kiša**
Study programme:	Applied Sciences in Engineering
Study branch:	Mathematical Engineering
Supervisor:	**doc. Ing. Petr Tomášek, Ph.D.**
Academic year:	2019/20

Pursuant to Act no. 111/1998 concerning universities and the BUT study and examination rules, you have been assigned the following topic by the institute director Master's Thesis:

Mathematical modelling of walking robots

Concise characteristic of the task:

Walking machines provide an important alternative to wheeled or tracked robots, as they are better suited to movement on uneven terrain, and in general are more versatile. Their design turns out to be much more complicated than in the case of wheeled or tracked robots. Many models of walking robots have been proposed, drawing inspiration from humans and other animals.

Goals Master's Thesis:

Walking robot model research.
Detailed analysis of the model.
Formulation and numerical solution of the robot motion optimal control problem.

Recommended bibliography:

WESTERVELT, E., GRIZZLE, J. W., CHEVALLEREAU, Ch., CHOI, J. H., MORRIS, B. Feedback Control of Dynamic Bipedal Robot Locomotion. CRC Press, Taylor & Francis Group, 2007, 28. DOI: 10.1201/9781420053739. ISBN 1420053728.

SPONG, M. W. a BHATIA, G. Further results on control of the compass gait biped. In: Proceedings 2003 IEEE/RSJ International Conference on Intelligent Robots and Systems (IROS 2003) (Cat. No.03CH37453) [online]. IEEE, 2003, 2, 1933-1938 vol.2 [cit. 2019-10-22]. DOI: 10.1109/IROS.2003.1248927. ISBN 0780378601.

GOSWAMI, A., ESPIAU, B. a KERAMANE, A. Limit Cycles in a Passive Compass Gait Biped and Passivity-Mimicking Control Laws. Autonomous Robots [online]. Boston: Kluwer Academic Publishers, 1997, 4(3), 273-286 [cit. 2019-10-25]. DOI: 10.1023/A:1008844026298. ISSN 0929-5593.

Deadline for submission Master's Thesis is given by the Schedule of the Academic year 2019/20

In Brno,

L. S.

prof. RNDr. Josef Šlapal, CSc. Director of the Institute	doc. Ing. Jaroslav Katolický, Ph.D. FME dean

Summary

This master's thesis deals with mathematical models of walking robots. Two such models are introduced. The rimless wheel, a passive precursor for other models, is studied analytically in detail. The compass gait biped model is analysed and simulated numerically in the Python programming language. A method for finding the conditions for passive gait of the biped is also implemented.

Abstrakt

Tato diplomová práce se zabývá matematickými modely kráčejících robotů. Dva z těchto modelů jsou vybrány a analyzovány. Pasivní model „rimless wheel“, který slouží jako základ pro další, složitější modely, je podrobně analyzován. „Compass gait“ model dvounohého robota je v práci analyzován a numericky simulován v programovacím jazyce Python. Metoda pro nalezení podmínek pro pasivní chůzi robota je rovněž implementována.

Keywords

robotics, mathematical modelling, compass gait, rimless wheel, dynamical systems, stability, Python, Poincaré map

Klíčová slova

robotika, matematické modelování, compass gait, rimless wheel, dynamické systémy, stabilita, Python, Poincarého zobrazení

KIŠA, Daniel. Matematické modelování kráčejících robotů. Brno, 2020. Dostupné také z: https://www.vutbr.cz/studenti/zav-prace/detail/124460. Diplomová práce. Vysoké učení technické v Brně, Fakulta strojního inženýrství, Ústav matematiky. Vedoucí práce Petr Tomášek.

I hereby declare that this thesis is my original work and that it has been written by me under the guidance of my supervisor doc. Ing. Petr Tomášek, Ph.D., using the sources listed in the references.

Daniel Kiša

I would like to express my sincerest thanks to the supervisor of my thesis, doc. Ing. Petr Tomášek, Ph.D. for his patience, kindness, valuable advice, and the time that he has spent helping me.

Daniel Kiša

Contents

1 Introduction

The capability of walking is one of humans' most underrated strengths. The deceiving simplicity of this exercise - most human babies are able to walk by the time they are 18 months old - hides the complex and highly nonlinear dynamics behind it. It is precisely these dynamics that make it very difficult to replicate the mechanisms of walking in robots.
However, the motivation for any such endeavours is clear. Compared with other ways of moving that utilize wheels, walking is much more versatile. Bipedal robots are able to move in places where wheeled robots would inherently struggle, such as areas with rough terrain. Another potential advantage of walking robots that should not be disregarded is that they are better suited for areas primarily designed for the movement of people, such as buildings or stairways.

The history behind the idea of constructing machines goes back to antiquity. First successes came in the 1960s, driven by a rapid development of related mathematical techniques and engineering. In 1967, the Waseda University based in Tokyo initiated the WABOT project which culminated six years later in WABOT-1, the world's first humanoid robot able to walk [1]. Since then, many similar projects have been undertaken by numerous teams at universities and private companies. Examples of these can be for instance the Massachusetts Institute of Technology Leg Laboratory founded by Marc Raibert in 1980 or the company Honda with its so-called P series - a progression of humanoid robot prototypes developed in the 1990s.
Around the same time, new, more aggressive approaches in the construction of legged robots relying on exploiting the mechanical system's passive dynamics started being investigated. In his seminal paper [2] written in 1990, McGeer examined the natural cyclic behavior of a collection of simple mechanical systems. He succeeded in popularizing the usage of techniques based on the study of Poincaré maps in the analysis of robotic systems.
Nowadays, the field of legged robotics is still undergoing rapid growth. The state of the art is exemplified in the works of companies such as Boston Dynamics and its Atlas robot, whose amazing acrobatic prowess displayed in various YouTube videos ([3][4]) can be appreciated by anyone with access to the Internet.

My interest in the subject was sparked in the year I spent at the University of L'Aquila as a part of a two-year Master's degree program. There, a friend of mine introduced me to the MIT course *Underactuated Robotics* taught by Russ Tedrake, whose lectures are readily available online [5]. My desire to learn and understand the course load led to the creation of this thesis. As a consequence, some unusual notational choices, such as defining the positive direction of an angle to be clockwise, have been made in compliance with this course.
The goal of the thesis is to give an introduction to the study of simple legged robots. Much of the literature that is available glosses over the techniques used to model such systems. For this reason, special care was given to a thorough explanation of these procedures. The proofs of the stated theorems were chosen so that they would not require a deep understanding of the theory. Indeed, cursory experience from an undergraduate course on dynamical systems is enough to follow the proofs.

The thesis consists of three major parts. In Section 2, mathematical foundations relevant to the main body of work are presented. This includes a brief introduction to the theory of dynamical systems with a couple of canonical examples. The notion of stability, which is fundamental for qualitative analysis of dynamical systems, is presented together with various definitions of stability used throughout the thesis. The Poincaré map - a link between the stability of continuous and discrete systems - is also introduced. The first section also contains a short summary of the Euler-Lagrange equations used to derive equations of motion for mechanical systems.
The second part is devoted to the rimless wheel model. The model and its assumptions are described and the equations of motion of its swing phase are derived. The mapping that governs its collision phase is also obtained. A Poincaré map for the system is defined and studied extensively. Its fixed points are identified for different possible arrangements of the model's parameters and their stability is treated as well. To conclude, the fixed points' regions of attraction are found and visualized.
The third part deals with the compass gait model. The readers is first introduced to its description and assumptions. Then, the system of differential equations governing its swing phase is obtained. The impact conditions and mapping are derived, too. In addition, a numerical solver of the hybrid system is implemented in Python. A Poincaré map for the system is defined analogically to the rimless wheel case and a search algorithm for its fixed points is demonstrated in Python. Both Python codes are included in the appendix.
In Section 5, the results of the thesis and possible future extensions are summarized.

2 Mathematical Background

2.1 Dynamical Systems

Many phenomena in science deal with quantites changing in time. Be it mechanical systems in physics, chemical reactions, or populations in biology, all of them can be described by the framework of dynamical systems. In essence, dynamical systems can be described by a state space (or phase space) and a rule that defines how they change in time.
In general, this scheme can have many different forms, but the two of the most typical examples are *continuous dynamical systems*, also called flows, where the rule is described by a system of differential equations

$$\dot{\mathbf{x}} = f(\mathbf{x}), \tag{2.1}$$

and *discrete dynamical systems* described by a system of difference equations

$$\mathbf{y}_{n+1} = f(\mathbf{y}_n), \qquad n = 0, 1, 2, \ldots \tag{2.2}$$

where $\mathbf{x}$ and $\mathbf{y}_n$ are elements of the respective systems' state spaces and f is a function from the state space to itself. Under some conditions on the function f, these rules imply that knowing the state of the system at one point in time uniquely determines the system's state at any other time in the future. Dynamical systems such as 2.1 and 2.2 where the function f does not explicitly depend on time are said to be *autonomous*.
Although the restriction to autonomous systems might seem too confining at first glance, any non-autonomous system can be turned into an autonomous one. As an example, consider the function on the right hand side of the differential equation (2.1) to be dependent on t as well. If we extend the state space by introducing a new state variable $\mathbf{x}_{n+1} = t$, we get rid of the time dependence simply by including the equation $\dot{\mathbf{x}}_{n+1} = 1$. It should be mentioned that this comes at the cost of adding an extra dimension to the state space. For more information, refer to [6].

To acquaint the reader with the subject, we present two typical examples of continuous and discrete dynamical systems.

Example 2.1 (Population growth)**.** Consider the simplest model of population growth described by the first-order differential equation

$$\dot{x} = rx,$$

where $x(t)$ is the population at time t, and $r > 0$ is the growth rate. If the equation is accompanied with an initial condition $x(0) = x_0$ determining the population at time 0, the solution can be written as

$$x(t) = x_0 e^{rt},$$

thus predicting an exponential growth. Even though the system is extremely simplistic, it can serve as a basis for other, more complex models. One of them is the so-called *logistic growth* model, which extends the idea of a simple exponential growth by introducing a carrying capacity of the population. The corresponding equation is given by

$$\dot{x} = rx\left(1 - \frac{x}{C}\right), \tag{2.3}$$

where the constant $C > 0$ is the aforementioned carrying capacity. The consequence of adding this parameter is that as x gets closer to C, the population growth slows rapidly. This continuous model has a famous discrete time counterpart, which brings us to to our second example.

Example 2.2 (Logistic map)**.** Consider the deceptively simple one-dimensional difference equation

$$y_{n+1} = r y_n \left(1 - y_n\right), \qquad n = 0, 1, 2, \ldots,$$

with $0 \leq r \leq 4$ and $y_0 \in (0, 1)$. Just like in the continuous case described in (2.3), we can consider y_n to carry the meaning of a population size. This elementary looking equation is often given as an example of how extraordinarily complicated behavior can arise out of nowhere. In particular, the system's character varies immensely for different values of the parameter r.
Let us fix the initial population y_0. When $0 < r < 1$, the population y_n eventually dies out. In contrast, for $1 < r < 3$, the population eventually approaches a nonzero steady state. However, as we keep increasing r, the population first starts periodically oscillating between two values, then four values, then $8, 16$, and so on. When r reaches approximately 3.56995, the system starts behaving *chaotically*. By this we mean that it exhibits great sensitivity to the initial condition y_0. We will formalize this kind of sensitivity by introducing the notion of *stability*. For more detail about the logistic map, see [6].

Before we proceed to the section about stability, we first mention the possibility of a dynamical system exhibiting the properties of a continuous system and a discrete system at the same time. Such systems are called *hybrid dynamical systems*. One important class of hybrid systems are *systems with impulse effects*. For such systems, the pair of a state space and a rule is extended by a subset S of the state space called the *switching surface*. The system's states then behave according to different rules, depending on if they lie on the switching surface or not. The rule can be summarized as

$$\begin{cases} \dot{\mathbf{x}} = f(\mathbf{x}), & \text{if } \mathbf{x} \notin S, \\ \mathbf{x}^+ = g(\mathbf{x}^-), & \text{if } \mathbf{x}^- \in S. \end{cases} \tag{2.4}$$

Example 2.3 (Bouncing ball)**.** An example of such a system can be the bouncing ball model. Consider a ball which is dropped from an initial height and which loses energy with each of its bounces. If by $x(t)$ we denote the ball's vertical position above the ground at time t, this model can be described by the relations

$$\begin{cases} \ddot{x} = -g, & \text{if } x > 0, \\ x^+ = x^-, \quad \dot{x}^+ = -\lambda \dot{x}^- & \text{if } x^- = 0. \end{cases}$$

Here, g is the gravitational acceleration and $\lambda > 0$ is a parameter describing the dissipation of the ball's energy at each bounce. An example of a numerical simulation of this model can be seen in [7].

2.2 Stability

The notion of stability is paramount in the study of dynamical systems. It is an example of a qualitative approach. Studying stability provides a way to increase one's understanding of the system without explicitly solving it - oftentimes such a solution is impossible to derive.
Many different approaches to stability may be considered. In this section, we state the definitions of stability used in the thesis. Before we do that, we introduce the concepts of equilibria and fixed points.

Definition 2.4. Consider the continuous dynamical system (2.1). We say that a state $\mathbf{x}$ is an *equilibrium point* of the system if $f(\mathbf{x}) = 0$.

Analogically, we define a fixed point of a discrete dynamical system.

Definition 2.5. Consider the discrete dynamical system (2.2). We say that a state $\mathbf{x}_n$ is a *fixed point* of the system if $f(\mathbf{x}_n) = \mathbf{x}_n$.

We proceed to define the various notions of stability used in the thesis.

Definition 2.6. Let (X, d) be a metric space. Consider the continuous dynamical system (2.1) and let $f : X \to X$ be continuous. We say that an equilibrium point $\mathbf{x} \in X$ is *stable in the sense of Lyapunov* if $\forall \varepsilon > 0,\ \exists \delta > 0$ such that $\forall \mathbf{y} \in X$ we have

$$d(\mathbf{x}, \mathbf{y}) < \delta \implies d(\mathbf{x}, \tilde{\mathbf{y}}(t)) < \varepsilon, \quad \forall t \in \mathbb{R},$$

where $\tilde{\mathbf{y}}(t)$ denotes the solution of (2.1) with the initial condition $\tilde{\mathbf{y}}(t) = \mathbf{y}$. We say that a fixed point $\mathbf{x} \in X$ is *unstable in the sense of Lyapunov* if it is not stable.

Remark. The symbol f^n in the definitions below represents an iteration of n compositions of the function f.

Definition 2.7. Let (X, d) be a metric space. Consider the discrete dynamical system (2.2) and let $f : X \to X$ be continuous. We say that a fixed point $\mathbf{x} \in X$ is *stable* if $\forall \varepsilon > 0,\ \exists \delta > 0$ such that $\forall \mathbf{y} \in X$ we have

$$d(\mathbf{x}, \mathbf{y}) < \delta \implies d(f^n(\mathbf{x}), f^n(\mathbf{y})) < \varepsilon, \quad \forall n \in \mathbb{N}.$$

We say that a fixed point $\mathbf{x} \in X$ is *unstable* if it is not stable.

Definition 2.8. Let (X, d) be a metric space. Consider the discrete dynamical system (2.2) and let $f : X \to X$ be continuous. We say that a fixed point $\mathbf{x} \in X$ is *asymptotically stable* if it is stable and if $\exists \delta > 0$ such that $\forall \mathbf{y} \in X$ we have

$$d(\mathbf{x}, \mathbf{y}) < \delta \implies \lim_{n \to \infty} d(f^n(\mathbf{x}), f^n(\mathbf{y})) = 0.$$

Definition 2.9. Let (X, d) be a metric space. Consider the discrete dynamical system (2.2) and let $f : X \to X$ be continuous. Let $\mathbf{x} \in X$ be asymptotically stable. We define the *region of attraction of* $\mathbf{x}$ to be the set of all points $\mathbf{y} \in X$ such that

$$\lim_{n \to \infty} d(f^n(\mathbf{x}), f^n(\mathbf{y})) = 0.$$

In the special case where $(X, d) = (\mathbb{R}, |\cdot|)$, we also introduce the notion of semistability.

Definition 2.10. Consider the discrete dynamical system (2.2) with the state space $\mathbb{R}$. Let $f : \mathbb{R} \to \mathbb{R}$ be a continuous function. We say that a point $x \in \mathbb{R}$ is *semistable* if $\forall \varepsilon > 0,\ \exists \delta > 0$ such that either $\forall y \in (-\infty, x)$, or $\forall y \in (x, \infty)$, we have

$$d(x, y) < \delta \implies d(f^n(x), f^n(y)) < \varepsilon, \quad \forall n \in \mathbb{N}.$$

We will distinguish the two different cases for y by calling x either *semistable from below* or *semistable from above*.

In the next section, we show how studying the stability of a continuous dynamical system can be rephrased into studying the stability of a discrete system.

2.3 Poincaré Map

One of the most common methods used for studying the stability of periodic orbits of dynamical systems makes use of the Poincaré map (also called the return map). The essence of the method lies in converting the problem of stability in the sense of Lyapunov of a *continuous* dynamical system's periodic solution to the problem of stability of a *discrete* dynamical system's fixed point. Refer to e.g. [8].

To explain the driving idea behind this approach (see [9]), we consider an autonomous equation in $\mathbb{R}^n$

$$\dot{\mathbf{x}} = f(\mathbf{x}). \tag{2.5}$$

Let $\tilde{\mathbf{x}}(t)$ be a periodic solution to this equation. Because the solution is periodic, it must correspond to a closed orbit Γ in the n-dimensional phase space. Let $\mathbf{x}_0 \in \Gamma$. Further, we construct an $(n-1)$-dimensional hyperplane Σ so that it is perpendicular to Γ and it passes through $\mathbf{x}_0$. If we then consider a point $\mathbf{x} \in \Sigma$ "close" to $\mathbf{x}_0$, the solution of (2.5) passing through $\mathbf{x}$ will again intersect Σ. The intersection of the solution with the hyperplane is denoted by $P(\mathbf{x})$. The mapping $P : \Sigma \to \Sigma$ is called the Poincaré map.

The requirement that Σ must be a hyperplane perpendicular to Γ can be easily generalized. In fact, it is sufficient to assume that Σ is an $(n-1)$-dimensional hypersurface *transversal* to Γ, where by transversality we mean that Σ is not tangent to Γ at $\mathbf{x}_0$. For more details, see [8].

In effect, by "cutting through" the phase space with Σ, we can identify orbits of (2.5) near Γ with points lying in Σ. Crucially, since Γ is a closed orbit, the point $\mathbf{x}_0$ is a fixed point of P. In other words,

$$P(\mathbf{x}_0) = \mathbf{x}_0.$$

The Lyapunov stability of the periodic solution $\tilde{\mathbf{x}}(t)$ then coincides with the stability of $\mathbf{x}_0$ according to Definition 2.7, with metric space $(X, d) = (\Sigma, d)$, where d is the usual Euclidean metric, and the function $f = P$.

Remark. In Definition 2.7, we require the function f to be continuous. The theorems establishing the Poincaré map's existence and continuity can be found in [8].

For the purposes of the thesis, this definition for continuous dynamical systems must be extended so that it encompasses systems with impulse effects defined in (2.4) as well. In such systems, a natural choice for Σ is the switching surface S. This question is treated in [10].

2.4 Euler-Lagrange Equations

For some mechanical systems, deriving the corresponding equations of motion is in its essence a simple task. Consider for example the one-dimensional system consisting of a point mass on the end of a linear spring. By applying Newton's second law of motion $F = ma$, we immediately arrive at the equation

$$m\ddot{x} = -kx,$$

where $x(t)$ measures the displacement of the point mass from the equilibrium position at time t. The problem is that this method does not scale well for larger, more complicated systems. In most applications, a different general scheme is required. This systematic approach was put together by the French-Italian mathematician Lagrange in his famous two volume treatise *Mécanique analytique*, first published in the years 1788 and 1789 (refer to [12]).

Lagrange's method is based on the calculus of variations, a field of mathematics concerned with finding the maxima and minima of functionals - mappings from a set of functions to the real numbers. As the scope of this thesis is too narrow to contain a reasonable treatment of the calculus of variations, we only mention (informally) the basic idea behind the Euler-Lagrange equations based on [11]. For a more in-depth description of Lagrangian mechanics, refer to [13].

Consider a mechanical system consisting of n point masses. Define the quantity L by

$$L = T - U,$$

where T and U are the sums of each of the point masses kinetic and potential energies, respectively. This quantity is called the *Lagrangian* of the system. Clearly,
$L = L(\mathbf{x}(t), \dot{\mathbf{x}}(t), t)$, where $\mathbf{x}(t)$ and $\dot{\mathbf{x}}(t)$ are the positions and velocities of each of the point masses at time t.
Now, consider the functional A (the so-called action) defined by

$$A(\mathbf{x}(t)) = \int_{t_1}^{t_2} L(\mathbf{x}(t), \dot{\mathbf{x}}(t), t),$$

and let $\mathbf{x}(t)$ be a function defined for $t \in [t_1, t_2]$ with its endpoints fixed. That is,
$\mathbf{x}(t_1) = \mathbf{x}_1, \mathbf{x}(t_2) = \mathbf{x}_2$. It can be shown that the functional A is *differentiable*. This means that

$$A(\mathbf{x}(t) + \mathbf{h}(t)) - A(\mathbf{x}(t)) = F(\mathbf{h}) + R(\mathbf{h}),$$

where F is linear in $\mathbf{h}$ and there exists positive constants ε and C such that

$$|\mathbf{h}| < \varepsilon \implies |R| \leq C\mathbf{h}^2.$$

The linear part $F(\mathbf{h})$ of the increment is then called the *differential* or the *variation* of the functional. A deeper explanation can be found in [13].

We state the following theorem without proof.

Theorem 2.11. Let $\mathbf{x}(t)$ be a function with its endpoints in t_1 and t_2 fixed that yields a stationary value of the functional A, where by stationary value we mean that its variation $F(\mathbf{h})$ is equal to zero. Then

$$\frac{d}{dt}\left[\frac{\partial L}{\partial \dot{\mathbf{x}}}\right] - \frac{\partial L}{\partial \mathbf{x}} = 0. \tag{2.6}$$

Combined with Hamilton's principle, which can be stated as *"The motion of a system of particles is the one that yields a stationary value of A"*, this implies that $\mathbf{x}(t)$ must satisfy (2.6).

The power of this method lies in the ease with which it can be used. Essentially, if one can find the kinetic and potential energies of the system, finding the equations of motion is only a routine question of taking a couple of derivatives.

Remark. It can be shown that the Euler-Lagrange equations are *independent* of the coordinate system. This means that they are valid for any coordinates describing the configuration of the mechanical system (these do not necessarily need to be the Cartesian coordinates). These are called *generalized coordinates* and are usually denoted by $\mathbf{q}(t)$. Their time derivatives $\dot{\mathbf{q}}(t)$ are called *generalized velocities*. The Euler-Lagrange equations (2.6) can be restated as

$$\frac{d}{dt}\left[\frac{\partial L}{\partial \dot{\mathbf{q}}}\right] - \frac{\partial L}{\partial \mathbf{q}} = 0. \tag{2.7}$$

To conclude this section, we note that the equations can be generalized to include the effects of external forces as well. If $W(\mathbf{q})$ is the work done by these forces, then the equation

$$\frac{d}{dt}\left[\frac{\partial L}{\partial \dot{\mathbf{q}}}\right] - \frac{\partial L}{\partial \mathbf{q}} = \frac{\partial W}{\partial \mathbf{q}} \tag{2.8}$$

must hold.

The mathematical apparatus introduced above will be used in solving various problems in the rest of the thesis.

3 The Rimless Wheel

One of the simplest models of walking is the so-called *rimless wheel*. It is an example of a passive walker - the system's movement is caused entirely by gravity and cannot be controlled. We will only concern ourselves with the 2D case of the model.
Consider a spoked wheel without the outer rim rolling down a ramp, with the spokes (or the legs) being evenly spaced. For simplicity, we assume the spokes to be rigid and all the mass to be concentrated in the center of the wheel. We further assume the spoke collisions to be perfectly inelastic and impulsive. Hence, the wheel loses some energy whenever one of its legs collides with the ground. We also do not consider the possibility of the stance leg slipping and assume the transfer of support to be instantaneous - there is no double-support phase.

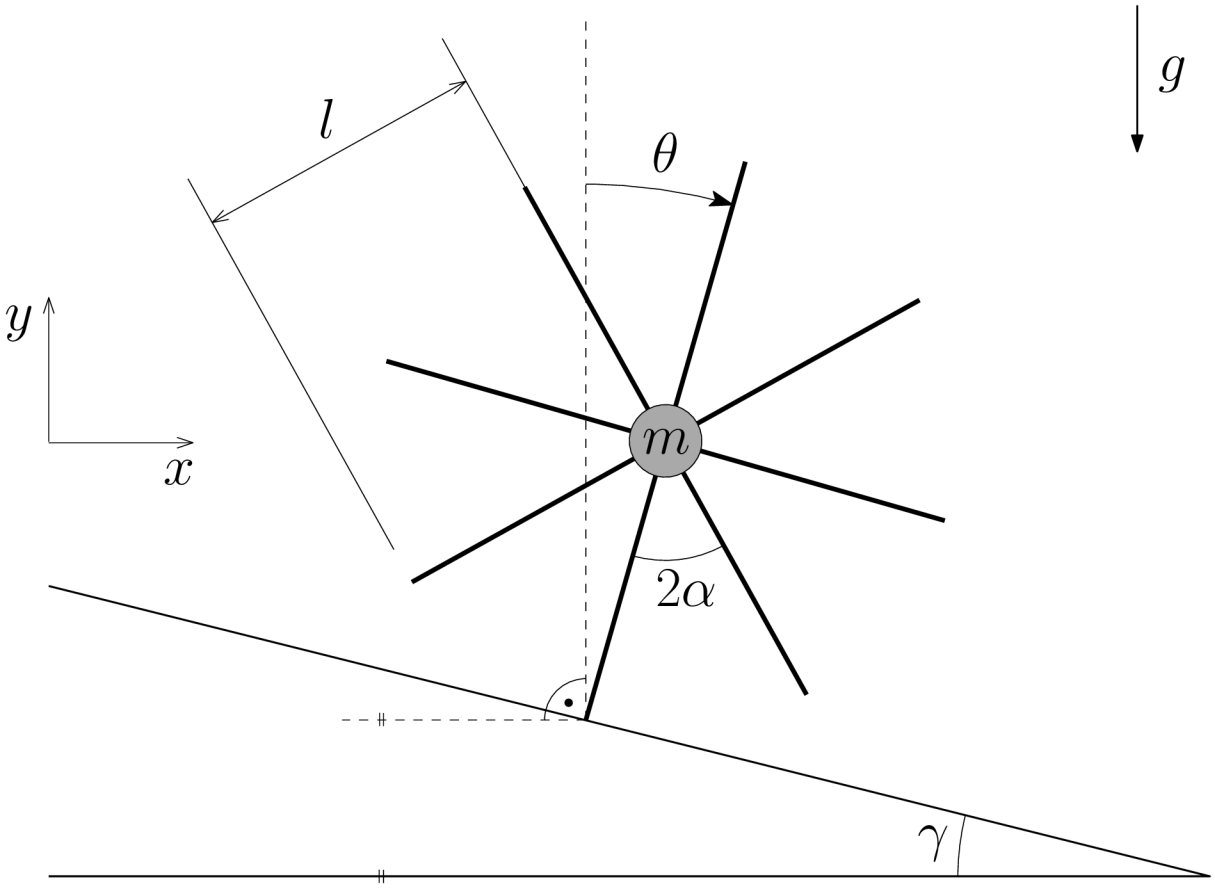

Figure 1. The rimless wheel model and the parameters that define it.

The model is completely specified by four parameters. These are the angle of the slope γ, the angle between two successive spokes 2α, the length of each spoke l and the wheel's mass m.
Natural assumptions on the parameters that govern the model can be made. Namely,

$$0 < \gamma < \frac{\pi}{2}, \qquad l > 0, \qquad g > 0, \qquad m > 0.$$

Remark. In fact, we could also allow $\gamma = 0$. However, it would introduce an additional special case for our analysis and hence we will only briefly comment on this possibility at the end of this section.

We also add an additional assumption on the number of spokes - we will restrict our work to wheels with at least 5 spokes. The reason for this is that with the assumptions outlined above, wheels with only 3 or 4 legs lose all of their energy upon collision and any further analysis is pointless. The condition of at least 5 legs can be written as

$$0 < \alpha < \frac{\pi}{4},$$

since if the number of spokes is n, then $\alpha = \frac{\pi}{n}$.
We will denote the region of admissible angles α and γ by $\Omega_{(\alpha,\gamma)}$.

$$\Omega_{(\alpha,\gamma)} = \left(0, \frac{\pi}{4}\right) \times \left(0, \frac{\pi}{2}\right). \tag{3.1}$$

The angle θ changes dynamically with time. In our model, it is taken to be a directed angle, with clockwise direction being positive, in accordance with [5]. While this is somewhat unusual, the choice of clockwise direction as the positive one stems from the fact that the ramp is sloped down from left to right. This way, as the wheel rolls down, the angle increases.

We split our analysis of the model into several parts. First, we will analyse the swing phase - the phase inbetween two collisions. We will derive the differential equation governing the swing phase and calculate the wheel's angular velocity just before next collision. Next, we will study the behavior of our system at the time of the collision. Combining these two, we will define a return map for the wheel's angular velocity just after the collision. Then, we will identify the fixed points of this map and discuss their stability, and at the end, we will specify their regions of attraction.

3.1 Swing Phase Model

To derive the differential equation governing the wheel's motion, we will use Lagrange's method. First, consider that the configuration of the wheel at time t depends solely on the angle of its stance leg. In other words, we do not distinguish between legs, they are all the same from the point of further analysis. Hence, we only have one generalized coordinate, namely $q(t) = \theta(t)$. We place the origin of the Cartesian coordinate system to the point where the stance leg is touching the ground. The position of the center of mass is then given by

$$\mathbf{x} = l \cdot \begin{bmatrix} \sin(\theta) \\ \cos(\theta) \end{bmatrix}.$$

Since all of the mass is assumed to be concentrated in the center, the wheel's kinetic energy (denoted by T) and potential energy (denoted by U) are given by

$$T = \frac{1}{2} m \dot{\mathbf{x}}^T \dot{\mathbf{x}} = \frac{1}{2} m l^2 \dot{\theta}^2,$$

$$U = mgx_2 = mgl\cos(\theta).$$

The Lagrangian function is defined in accordance with Subsection 2.4 as

$$L = T - U$$

and the Euler-Lagrange equations take the form of

$$\frac{\partial L}{\partial \theta} - \frac{d}{dt}\left[\frac{\partial L}{\partial \dot{\theta}}\right] = mgl\sin(\theta) - \frac{d}{dt}\left[ml^2\dot{\theta}\right] = 0$$

$$\ddot{\theta} = \frac{g}{l}\sin(\theta), \tag{3.2}$$

which is the well-known equation of a simple pendulum.

Remark. This is a nonlinear second order differential equation. A closed-form solution can be found (see for example [14]), but its derivation is quite technical and since it does not really bear on the rest of our analysis, we omit it completely. Of course, given initial conditions, it is trivial to find an approximate solution numerically.

In the next step, we wish to describe the angular velocity of the wheel at the end of the swing phase (just before the next collision) with respect to the beginning of the swing phase (just after the previous collision). Before we proceed, we must find the value of the state variable θ before and after the collision. We denote these by $\theta(0^-)$ and $\theta(0^+)$, respectively. In the same way, we introduce the angular velocities $\dot{\theta}(0^-)$ and $\dot{\theta}(0^+)$. By a simple geometrical argument presented in Fig. 2, we find that

$$\theta(0^-) = \gamma + \alpha,$$

$$\theta(0^+) = \gamma - \alpha.$$

The first diagram represents the configuration just before the collision. The second one captures the situation right after the collision. As the stance leg changes, so must the configuration.

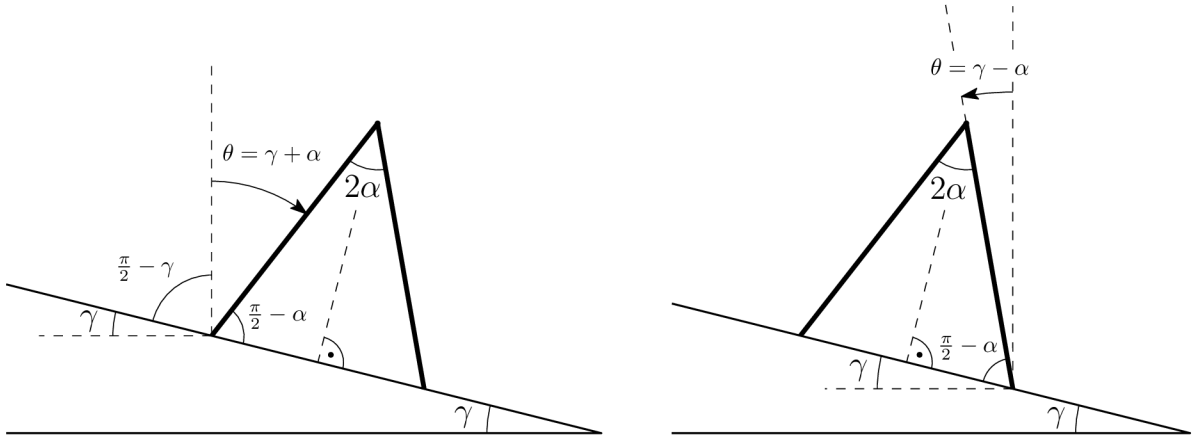

Figure 2. The two situations showing the wheel's state a moment before and after a collision.

Remark. We can see that θ only changes by 2α along the wheel's whole swing. As the number of legs increases, α becomes smaller and the equation (3.2) can in fact be linearized around $\theta = \gamma$. The question of finding its solution then dramatically simplifies.

Given an initial positive angular velocity $\dot{\theta}(0^+) = \omega$, we would like to derive an expression for the final angular velocity $\dot{\theta}(0^-)$. First, we must distinguish between two distinct cases. If ω is too small, the wheel will not have enough energy to vault its mass over the point of maximum potential energy, that is, $\theta = 0$. In that case, it is going to slowly reverse direction and come back to its initial configuration $\theta = \gamma - \alpha$ with $\dot{\theta} = -\omega$.
This happens because in our considerations, the wheel conserves energy during the swing phase. In the second case, the wheel has enough energy to carry its mass over the critical point and it completes one full step. Next, we calculate exactly the critical value of ω that is needed for the second case to be true.

We do this by means of analysing the wheel's energy. At time $t = 0^+$, the kinetic and potential energies are given by

$$T = \frac{1}{2} m l^2 \omega^2$$

$$U = mgl \cos\left(\theta(0^+)\right) = mgl \cos\left(\gamma - \alpha\right).$$

The total energy is given as the sum of these two values.

$$E = T + U = \frac{1}{2} m l^2 \omega^2 + mgl \cos\left(\gamma - \alpha\right)$$

This value must be constant during the whole swing phase. Now, the potential energy is maximized at the highest point of the swing (the stance leg being vertical). It is given by

$$U^* = mgl \cos\left(0\right) = mgl.$$

If the wheel has greater total energy than this critical value, it will be able to complete a step. This condition can be expressed followingly.

$$E(0^+) > U^*$$

$$\frac{1}{2} m l^2 \omega^2 + mgl \cos\left(\gamma - \alpha\right) > mgl$$

By simplifying and expressing ω, we obtain

$$\omega > \sqrt{2\frac{g}{l}(1 - \cos(\gamma - \alpha))}. \tag{3.3}$$

This condition is valid for the case $\gamma \leq \alpha$. In the special case of $\gamma = \alpha$, this condition reduces to the simple

$$\omega > 0.$$

However, the condition (3.3) is invalid for $\gamma > \alpha$, as in that case the center of mass at time $t = 0^+$ is already over the critical point and hence the wheel will always make a step forward.

Remark. The expression in the condition (3.3) comes up frequently in subsequent text and hence we decided to denote it by

$$\omega_f = \sqrt{2\frac{g}{l}(1 - \cos(\gamma - \alpha))}. \tag{3.4}$$

The subscript f stands for *forward*.

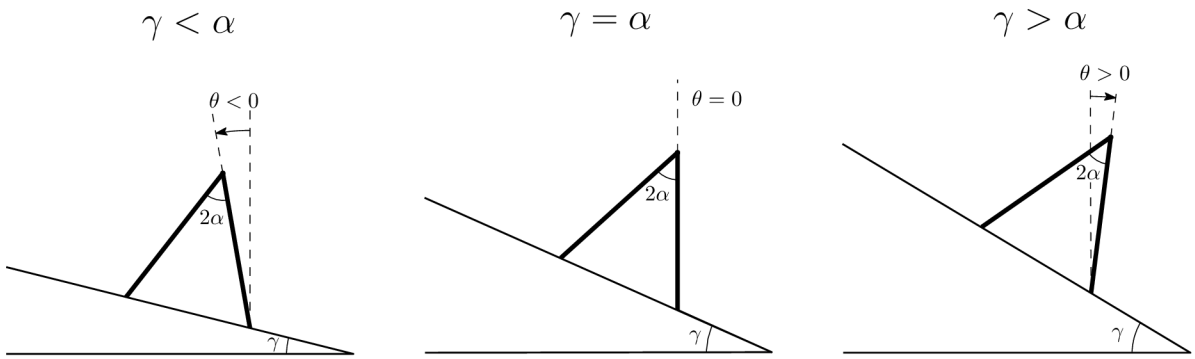

Figure 3. The positions of the wheel's legs at the moment of collision for $\gamma < \alpha$, $\gamma = \alpha$, and $\gamma > \alpha$ respectively. Note that for $\gamma > \alpha$, the center of mass is already over the critical line $\theta = 0$.

Next, we would like to express the angular velocity at the end of the step as a function of ω. We will again use the fact that energy is conserved. We will denote the final angular velocity by $\dot{\theta}(t^-)$. The energy in the initial and final state must be equal. This gives us

$$E(0^+) = E(t^-),$$

$$\frac{1}{2}ml^2\omega^2 + mgl\cos(\gamma - \alpha) = \frac{1}{2}ml^2\dot{\theta}^2(t^-) + mgl\cos(\gamma + \alpha).$$

By dividing by ml and rearranging, we get

$$\frac{1}{2}l\dot{\theta}^2(t^-) = \frac{1}{2}l\omega^2 + g(\cos(\gamma - \alpha) - \cos(\gamma + \alpha)).$$

Now, we apply the formulas for the sum and difference of two angles and obtain

$$\frac{1}{2}l\dot{\theta}^2(t^-) = \frac{1}{2}l\omega^2 + 2g\sin(\gamma)\sin(\alpha).$$

Finally, we express $\dot{\theta}(t^-)$ for ω satisfying (3.3).

$$\dot{\theta}(t^-) = \sqrt{\omega^2 + 4\frac{g}{l}\sin(\gamma)\sin(\alpha)}. \tag{3.5}$$

3.1.1 Backward Motion

Before we proceed further, we extend our previous work to include the possibility of moving in the other direction, that is, up the ramp. The analysis is identical to one done before for the wheel rolling down, just with different initial conditions for our differential equation. Here, $\theta(0^+) = \gamma + \alpha$ and $\dot{\theta}(0^+) = -\omega$, where $\omega > 0$.
As not to repeat the same calculations, we only state the results. We arrive at a condition similar to (3.3) for making a full step up the ramp.

$$\dot{\theta}(0^+) = -\omega < -\sqrt{2\frac{g}{l}(1 - \cos(\gamma + \alpha))}. \tag{3.6}$$

This condition is required for all possible arrangements of γ and α, as for moving up the ramp, it can never happen that the center of mass is already over the vertical line $\theta = 0$.

Remark. Similarly to the forward motion case, for further clarity we denote

$$\omega_b = -\sqrt{2\frac{g}{l}(1 - \cos(\gamma + \alpha))}. \tag{3.7}$$

The subscript b stands for *backward*.

Once again, we also derive the formula for the final angular velocity depending on ω, following the same steps as in the forward motion case.

$$\dot{\theta}(t^-) = \sqrt{\omega^2 - 4\frac{g}{l}\sin(\gamma)\sin(\alpha)}. \tag{3.8}$$

3.1.2 Rocking Motion

Here, we complete our analysis by considering the last possible option for ω, i.e. the case when it does not satisfy either of the conditions (3.3) and (3.6). This can be expressed as

$$\omega_b < \dot{\theta} < \omega_f. \tag{3.9}$$

This means that the wheel does not have enough energy and after its center reaches its highest point, it slowly comes back to its initial state with the angular velocity reversed.

$$\dot{\theta}(t^-) = -\dot{\theta}(0^+). \tag{3.10}$$

This concludes our investigation of the swing phase model.

3.2 Collision Analysis

In this section, we will study what happens at the time when the wheel's next leg collides with the ground. At that point, we come to a discontinuity that we must fully understand and describe. For one, the stance leg and together with it the angle θ describing the wheel's configuration are changed. In addition, the collision does not conserve energy, there is some dissipation present. However, since we assume collisions to be perfectly inelastic and impulsive, we know that angular momentum must be conserved. We will use this to calculate the change in angular velocity.
By $\mathbf{L}(t^-)$ and $\mathbf{L}(t^+)$ we denote the angular momentum around the point of collision just before and after the leg hits the ground, respectively. These two momenta must be equal.

We begin by calculating $\mathbf{L}(t^-)$.
To do this, we first move the origin of our coordinate system to the point of collision and then calculate the position and velocity of the center of mass (denoted by $\mathbf{x}_c$, $\dot{\mathbf{x}}_c$). It can be shown that

$$\mathbf{x}_c = 2l\sin(\alpha)\cdot\begin{bmatrix}-\cos(\gamma)\\ \sin(\gamma)\end{bmatrix} + l\cdot\begin{bmatrix}\sin(\theta(t^-))\\ \cos(\theta(t^-))\end{bmatrix}.$$

If we substitute $\theta(t^-) = \gamma + \alpha$, we get

$$\mathbf{x}_c = l\cdot\begin{bmatrix}-2\sin(\alpha)\cos(\gamma)+\sin(\gamma+\alpha)\\ 2\sin(\alpha)\sin(\gamma)+\cos(\gamma+\alpha)\end{bmatrix} = l\cdot\begin{bmatrix}\sin(\gamma-\alpha)\\ \cos(\gamma-\alpha)\end{bmatrix}.$$

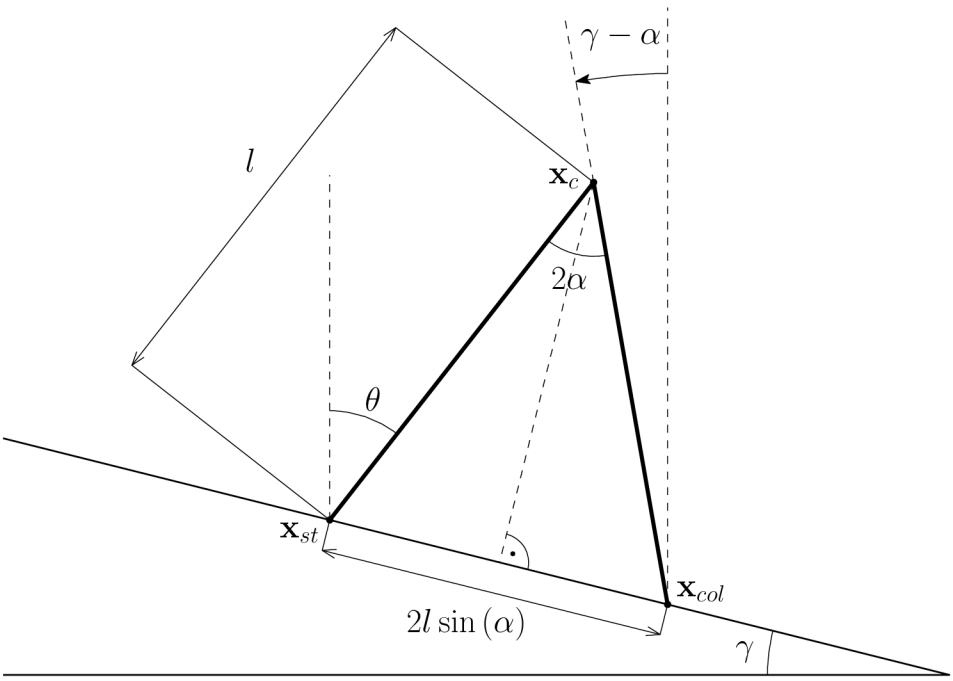

Figure 4. The situation just before the collision. Here, $\mathbf{x}_{st}$ represents the point where the stance leg is touching the ground, $\mathbf{x}_{col}$ the point where the next leg is going to collide with the ground, and $\mathbf{x}_c$ the wheel's center of mass. Clearly, $\mathbf{x}_c = \mathbf{x}_{st} + (\mathbf{x}_c - \mathbf{x}_{st})$.

We obtain $\dot{\mathbf{x}}_c$ by differentiating the first expression for $\mathbf{x}_c$ with respect to time.

$$\dot{\mathbf{x}}_c = l\dot{\theta}(t^-) \cdot \begin{bmatrix} \cos\left(\theta(t^-)\right) \\ -\sin\left(\theta(t^-)\right) \end{bmatrix} = l\dot{\theta}(t^-) \cdot \begin{bmatrix} \cos\left(\gamma+\alpha\right) \\ -\sin\left(\gamma+\alpha\right) \end{bmatrix}.$$

Now, we apply the well-known formula $\mathbf{L}(t^-) = \mathbf{x}_c \times m\dot{\mathbf{x}}_c$ (see Subsection. The momentum is then equal to

$$\mathbf{L}(t^-) = \hat{\mathbf{k}} \left(l\sin\left(\gamma-\alpha\right) \cdot \left(-ml\dot{\theta}(t^-)\sin\left(\gamma+\alpha\right)\right) - l\cos\left(\gamma-\alpha\right) \cdot ml\dot{\theta}(t^-)\cos\left(\gamma+\alpha\right) \right),$$

where $\hat{\mathbf{k}}$ represents the vector $[0,0,1]^T$.
By rearranging and using the formula for the cosine of a difference of two angles, this can be simplified to

$$\mathbf{L}(t^-) = -\hat{\mathbf{k}}ml^2\dot{\theta}(t^-)\cos\left(2\alpha\right).$$

By doing the exact same analysis for the instant right after the collision $t = t^+$, we derive the new position and velocity of the center of mass.

$$\mathbf{x}_c = l \cdot \begin{bmatrix} \sin\left(\gamma-\alpha\right) \\ \cos\left(\gamma-\alpha\right) \end{bmatrix}.$$

$$\dot{\mathbf{x}}_c = l\dot{\theta}(t^+) \cdot \begin{bmatrix} \cos\left(\gamma-\alpha\right) \\ -\sin\left(\gamma-\alpha\right) \end{bmatrix}.$$

The new angular momentum is given by

$$\mathbf{L}(t^+) = -\hat{\mathbf{k}}ml^2\dot{\theta}(t^+).$$

By setting the two momenta to be equal, we can express the new angular velocity after impact $\dot{\theta}(t^+)$ in terms of $\dot{\theta}(t^-)$.

$$\dot{\theta}(t^+) = \dot{\theta}(t^-)\cos\left(2\alpha\right). \tag{3.11}$$

This formula represents the loss of velocity due to dissipation of energy (notice that $\cos\left(2\alpha\right)$ is always less or equal to 1).

Remark. The loss of energy can be expressed as

$$\begin{aligned} E(t^+) - E(t^-) &= T(t^+) - T(t^-) \\ &= \frac{1}{2}ml^2\dot{\theta}^2(t^+) - \frac{1}{2}ml?^2\dot{\theta}^2(t^-) \\ &= \frac{1}{2}ml^2\cos^2\left(2\alpha\right)\dot{\theta}^2(t^-) - \frac{1}{2}ml^2\dot{\theta}^2(t^-) \\ &= -\frac{1}{2}ml^2\dot{\theta}^2(t^-) \cdot \left(1-\cos^2\left(2\alpha\right)\right) \\ &= -\frac{1}{2}ml^2\sin^2\left(2\alpha\right)\dot{\theta}^2(t^-). \end{aligned} \tag{3.12}$$

3.3 Long-Term Behavior

So far, we have only studied a small moment in the wheel's motion - what happens in the process of making one "step". The question of what happens as time goes on is much more interesting. To answer it, we first introduce a Poincaré map for the angular velocity at the beginning of each step and thus obtain a discrete dynamical system. We can then investigate its properties, such as fixed points and stability.

3.3.1 The Poincaré Map

We introduce a mapping from the angular velocity at the start of the n^{th} cycle to the start of the next one. Each cycle consists of a swing phase and a collision. In our investigation of the swing phase, we derived formulas (3.5), (3.8), and (3.10) for the angular velocity at the end of the swing in terms of the velocity at the start of it. Also, as we have established earlier (see formula (3.11)),

$$\dot{\theta}(t^+) = \cos(2\alpha)\dot{\theta}(t^-).$$

By bringing this together, we are ready to define the mapping. By $\dot{\theta}_n$, we denote the angular velocity at the start of the n^{th} cycle. We split the definition into two cases, $\gamma \leq \alpha$ and $\gamma > \alpha$, as there are qualitative differences between them.
For $\gamma \leq \alpha$, we have

$$\dot{\theta}_{n+1} = \begin{cases} \cos(2\alpha)\sqrt{\dot{\theta}_n^2 + 4\frac{g}{l}\sin(\gamma)\sin(\alpha)} & \text{for } \dot{\theta}_n > \omega_f \\ -\cos(2\alpha)\dot{\theta}_n & \text{for } \omega_b < \dot{\theta}_n < \omega_f \\ -\cos(2\alpha)\sqrt{\dot{\theta}_n^2 - 4\frac{g}{l}\sin(\gamma)\sin(\alpha)} & \text{for } \dot{\theta}_n < \omega_b. \end{cases} \tag{3.13}$$

Notice that the map is not defined for $\dot{\theta}_n$ being equal to one of the critical values ω_f and ω_b that disconnect the definition. This is because for those values of $\dot{\theta}_n$, the state variables θ and $\dot{\theta}$ are moving along a heteroclinic orbit towards the unstable equilibrium $\theta = 0$, $\dot{\theta} = 0$. This takes infinite amount of time and so the $(n+1)^{th}$ cycle never happens and hence the map cannot be defined.
For $\gamma > \alpha$, the condition (3.3) disappears and hence we define the map as follows.

$$\dot{\theta}_{n+1} = \begin{cases} \cos(2\alpha)\sqrt{\dot{\theta}_n^2 + 4\frac{g}{l}\sin(\gamma)\sin(\alpha)} & \text{for } \dot{\theta}_n \geq 0 \\ -\cos(2\alpha)\dot{\theta}_n & \text{for } \omega_b < \dot{\theta}_n < 0 \\ -\cos(2\alpha)\sqrt{\dot{\theta}_n^2 - 4\frac{g}{l}\sin(\gamma)\sin(\alpha)} & \text{for } \dot{\theta}_n \leq \omega_b. \end{cases} \tag{3.14}$$

In this case, the unstable equilibrium $\theta = 0$, $\dot{\theta} = 0$ is unreachable, because the wheel's center of mass is over its maximum potential energy state at all times (see Fig. 3). Thus, the issue with heteroclinic orbits is not present. This allows us to extend the definition to the two critical angular velocities ω_f and ω_b.
Now, given a pair of initial data $(\theta, \dot{\theta})$, we can use this recursive definition to say what the wheel will do in the n^{th} cycle. This gives us the apparatus for describing its long-term behavior.

3.3.2 Some Properties of the Poincaré Map

The natural question that immediately arises is that of deriving a closed-form expression from our recursive definition. Owing to the inherent disconnectedness of the map, this is only partially possible. Nevertheless, even these partial results will be of considerable help later. In this section, we state and prove some of them.
We define $\dot{\theta}_{n+m}$ to be the angular velocity after m cycles, starting from $\dot{\theta}_n$. We begin with the "backward motion" regime, where the wheel is moving up the ramp.

Lemma 3.1. Let $m \in \mathbb{N}$ and

$$\dot{\theta}_{n+i} < \omega_b, \quad \forall i \in \{0, 1, 2, \ldots, m-1, m\}.$$

Then

$$\dot{\theta}_{n+m} = -\cos(2\alpha)\sqrt{\cos^{2(m-1)}(2\alpha) \cdot \dot{\theta}_n^2 - 4\frac{g}{l}\sin(\gamma)\sin(\alpha) \cdot \frac{1-\cos^{2m}(2\alpha)}{1-\cos^2(2\alpha)}}. \tag{3.15}$$

Proof. We prove this by induction. For $m = 1$, this statement is equivalent to

$$\dot{\theta}_{n+1} = -\cos(2\alpha)\sqrt{\dot{\theta}_n^2 - 4\frac{g}{l}\sin(\gamma)\sin(\alpha)}$$

which is true by the map's definition (either (3.13) or (3.14)). We assume it is true for $m = k$ and show that it then must be true for $m = k + 1$. By our definition we have

$$\dot{\theta}_{n+k+1} = -\cos(2\alpha)\sqrt{\dot{\theta}_{n+k}^2 - 4\frac{g}{l}\sin(\gamma)\sin(\alpha)}.$$

We use the formula for a partial sum of the geometric series

$$\frac{1-\cos^{2k}(2\alpha)}{1-\cos^2(2\alpha)} = \sum_{i=0}^{k-1}\cos^{2i}(2\alpha)$$

and substitute our induction hypothesis. We obtain

$$\dot{\theta}_{n+k+1} = -\cos(2\alpha)\cdot$$
$$\left(\cos^2(2\alpha)\left(\cos^{2(k-1)}(2\alpha)\cdot\dot{\theta}_n^2 - 4\frac{g}{l}\sin(\gamma)\sin(\alpha)\cdot\sum_{i=0}^{k-1}\cos^{2i}(2\alpha)\right)^2 - 4\frac{g}{l}\sin(\gamma)\sin(\alpha)\right)^{\frac{1}{2}}.$$

By distributing $\cos^2(2\alpha)$ inside the bracket and simplifying, we get

$$\dot{\theta}_{n+k+1} = -\cos(2\alpha)\sqrt{\cos^{2k}(2\alpha)\cdot\dot{\theta}_n^2 - 4\frac{g}{l}\sin(\gamma)\sin(\alpha)\cdot\sum_{i=0}^{k}\cos^{2i}(2\alpha)}.$$

After using the partial sum formula one last time, we arrive at exactly the formula (3.15) for $m = k + 1$ and the proof is done.

□

Next, we attempt find a closed formula for the other time direction, in a sense, asking the question what the angular velocity would have to look like m steps ago, given that we know $\dot{\theta}_n$. We define $\dot{\theta}_{n-m}$ to be such angular velocity that after m cycles it is exactly equal to $\dot{\theta}_n$.

Lemma 3.2. Let $m \in \mathbb{N}$ and

$$\dot{\theta}_{n-i} < \omega_b, \quad \forall i \in \{0, 1, 2, \ldots, m-1, m\}.$$

Then

$$\dot{\theta}_{n-m} = -\sqrt{\cos^{-2m}(2\alpha) \cdot \dot{\theta}_n^2 + 4\frac{g}{l}\sin(\gamma)\sin(\alpha) \cdot \frac{1 - \cos^{-2m}(2\alpha)}{1 - \cos^{-2}(2\alpha)}}.$$

Proof. To prove that this is true, we will use the result of Lemma 3.1. Using that formula, it is sufficient to show that

$$\dot{\theta}_n = -\cos(2\alpha)\sqrt{\cos^{2(m-1)}(2\alpha) \cdot \dot{\theta}_{n-m}^2 - 4\frac{g}{l}\sin(\gamma)\sin(\alpha) \cdot \frac{1 - \cos^{2m}(2\alpha)}{1 - \cos^2(2\alpha)}}$$

holds. After substituting the formula for $\dot{\theta}_{n-m}$ into this expression and simplifying, we arrive at

$$\dot{\theta}_n = -\cos(2\alpha) \cdot \sqrt{\cos^{-2}(2\alpha) \cdot \dot{\theta}_n^2 + 4\frac{g}{l}\sin(\gamma)\sin(\alpha) \cdot \left(\frac{\cos^{2(m-1)}(2\alpha) - \cos^{-2}(2\alpha)}{1 - \cos^{-2}(2\alpha)} - \frac{1 - \cos^{2m}(2\alpha)}{1 - \cos^2(2\alpha)}\right)}.$$

But since $1 - \cos^{-2}(2\alpha) = -\cos^{-2}(2\alpha) \cdot (1 - \cos^2(2\alpha))$, the bracket multiplying the term $4\frac{g}{l}\sin(\gamma)\sin(\alpha)$ vanishes and we obtain

$$\dot{\theta}_n = -\sqrt{\dot{\theta}_n^2} = -|\dot{\theta}_n|,$$

which is clearly true because we assume $\dot{\theta}_n$ to be negative.

□

Now, we turn our attention to the "rocking" regime. We have to distinguish between the cases $\gamma \leq \alpha$ and $\gamma > \alpha$, but the formulas themselves are much simpler. In fact, we can unify the formulas for both time directions into one expression.

Lemma 3.3. Let $m \in \mathbb{Z}$. Let either

$$\omega_b < \dot{\theta}_{n+i} < \omega_f \qquad \text{for } \gamma \leq \alpha$$

or

$$\omega_b < \dot{\theta}_{n+i} < 0 \qquad \text{for } \gamma > \alpha,$$

$\forall\, i \in \{m, m+1, ..., 0\}$ if $m < 0$, or $\forall\, i \in \{0, 1, ..., m\}$ if $m \geq 0$. Then

$$\dot{\theta}_{n+m} = (-1)^m \cos^m(2\alpha)\dot{\theta}_n.$$

Proof. Similarly to the proofs above, this can be easily done by using inductive reasoning.

□

Finally, we set our eyes toward the "forward" direction.

Lemma 3.4. Let $m \in \mathbb{N}$. Let

$$\dot{\theta}_{n+i} > \omega_f \qquad \text{for } \gamma \leq \alpha$$

or

$$\dot{\theta}_{n+i} \geq 0 \qquad \text{for } \gamma > \alpha,$$

$\forall\ i \in \{0, 1, 2, ..., m-1, m\}$. Then

$$\dot{\theta}_{n+m} = \cos(2\alpha)\sqrt{\cos^{2(m-1)}(2\alpha) \cdot \dot{\theta}_n^2 + 4\frac{g}{l}\sin(\gamma)\sin(\alpha) \cdot \frac{1-\cos^{2m}(2\alpha)}{1-\cos^2(2\alpha)}}.$$

Proof. The proof of this statement is completely identical to the proof of Lemma 3.1. □

Lemma 3.5. Let $m \in \mathbb{N}$. Let

$$\dot{\theta}_{n-i} > \omega_f \qquad \text{for } \gamma \leq \alpha$$

or

$$\dot{\theta}_{n-i} \geq 0 \qquad \text{for } \gamma > \alpha,$$

$\forall\ i \in \{0, 1, 2, ..., m-1, m\}$. Then

$$\dot{\theta}_{n-m} = \sqrt{\cos^{-2m}(2\alpha) \cdot \dot{\theta}_n^2 - 4\frac{g}{l}\sin(\gamma)\sin(\alpha) \cdot \frac{1-\cos^{-2m}(2\alpha)}{1-\cos^{-2}(2\alpha)}}.$$

Proof. The proof of this statement is completely identical to the proof of Lemma 3.2. □

Before proceeding to the next section, we must deal with the issue of heteroclinic orbits arising when $\gamma \leq \alpha$. We do this now to avoid running into trouble later. In the event that the system enters one of these pathological orbits, our definition of the Poincaré map (refer to (3.13)) essentially breaks down.

Definition 3.6. Let $\gamma \leq \alpha$. We define the *sets of heteroclinic orbits* (denoted by H_1 and H_2) to be the sets of angular velocities such that after a finite number of steps, they reach the heteroclinic orbits ω_b and ω_f, respectively.

$$H_1 := \{\dot{\theta}_n \in \mathbb{R} \mid \exists m \in \mathbb{N} : \dot{\theta}_{n+m} = \omega_b\}.$$
$$H_2 := \{\dot{\theta}_n \in \mathbb{R} \mid \exists m \in \mathbb{N} : \dot{\theta}_{n+m} = \omega_f\}.$$

In addition, we define their union H.

$$H := H_1 \cup H_2.$$

As we can see, both sets H_1 and H_2 are countable and thus have measure 0 in $\mathbb{R}$. Practically speaking, they do not have an influence on the wheel's behavior, but we include them with the purpose of having our analysis as complete as possible.

Remark. If $\gamma \leq \alpha$ and $\dot{\theta}_n \in H$, then the limit $\lim_{m\to\infty} \dot{\theta}_{n+m}$ does not exist.

3.3.3 Fixed Points Existence

By the Poincaré map's fixed point, we mean an angular velocity ω^* satisfying

$$\dot{\theta}_{n+1} = \dot{\theta}_n = \omega^*.$$

These points are of great importance because they represent repeating cycles of the same motion - a powerful tool for predicting how the wheel is going to behave. We begin by establishing the conditions for their existence. As we have two different definitions for the Poincaré map, we again split the analysis in two cases.
For $\gamma \leq \alpha$, it is easy to see that there is always the fixed point

$$\omega^* = 0$$

for the reason that if $\dot{\theta}_n = 0$, then, according to (3.13) and (3.14),

$$\dot{\theta}_{n+1} = -\cos(2\alpha) \cdot 0 = 0.$$

This fixed point represents the wheel being stopped with two legs touching the ground and supporting it and we will denote the fixed point by ω^*_{stop}.
Next, we will investigate the possibility of the existence of a fixed point ω^* satisfying (3.3). This would represent rolling down the ramp at "constant speed". From the definition of our return map (see (3.13), (3.14)), we get the equation

$$\omega^* = \cos(2\alpha)\sqrt{\omega^{*2} + 4\frac{g}{l}\sin(\gamma)\sin(\alpha)}.$$

By raising both sides of the equation to the second power and distributing $\cos^2(2\alpha)$ over all other terms, we obtain

$$\omega^{*2}(1 - \cos^2(2\alpha)) = 4\frac{g}{l}\cos^2(2\alpha)\sin(\gamma)\sin(\alpha).$$

We use the fact that $1 - \cos^2(2\alpha) = \sin^2(2\alpha)$, we divide by it and then take the square root of both sides.

$$\omega^* = 2\cot(2\alpha)\sqrt{\frac{g}{l}\sin(\gamma)\sin(\alpha)}.$$

Taking the root is justified because in our model we assume the wheel to have at minimum five legs, which gives $\alpha < \frac{\pi}{4}$ and thus $\cot(2\alpha) > 0$, $\sin(\alpha) > 0$. Because we are in the case of $\gamma \leq \alpha$, also $\sin(\gamma) > 0$.
It needs to be emphasized that this fixed point only exists when ω^* actually satisfies (3.3), that is,

$$2\cot(2\alpha)\sqrt{\sin(\gamma)\sin(\alpha)} > \sqrt{2(1 - \cos(\gamma - \alpha))} \tag{3.16}$$

must be satisfied. The validity of this inequality depends solely on the parameters α and γ of our model. We denote this fixed point by ω^*_{roll}.

Lastly, we check the possibility of the existence of a fixed point for moving up the ramp. Going through the same procedure as above, just for the equation

$$\omega^* = -\cos(2\alpha)\sqrt{\omega^{*2} - 4\frac{g}{l}\sin(\gamma)\sin(\alpha)},$$

we obtain

$$0 < \omega^{*2} = -4\cot^2(2\alpha)\frac{g}{l}\sin(\gamma)\sin(\alpha) < 0$$

and thus a contradiction. This makes sense intuitively, it should not be possible for the wheel to be moving up the ramp indefinitely as it is losing speed both from the collisions and in the swing phases.
To conclude, in the case of $\gamma \leq \alpha$, the return map has either one or two fixed points. There is always ω^*_{stop} corresponding to the wheel standing on two of its legs, and for parameters satisfying (3.16), there is also ω^*_{roll} corresponding to the wheel rolling down at constant speed.
For $\gamma > \alpha$, the situation is a bit different. Here, the fixed point $\omega^*_{stop} = 0$ vanishes because by our definition of the Poincaré map (see (3.14)),

$$\dot{\theta}_{n+1} = -\cos(2\alpha)\dot{\theta}_n$$

is only valid for $\dot{\theta}_n < 0$. In other words, the slope is too steep for the wheel to stand on two legs.
However, ω^*_{roll} is still present, and contrary to the previous case, it has no extra condition depending on the parameters. For $\gamma > \alpha$, it always exists.

3.3.4 Fixed Points Stability

In this section we investigate the stability of our fixed points in accordance with our definitions 2.7 and 2.8. We will start with proving the following results.

Lemma 3.7. Let $0 < \alpha < \frac{\pi}{4}$, $0 < \gamma < \frac{\pi}{2}$. Then the inequalities

$$2\cot(2\alpha)\sqrt{\sin(\gamma)\sin(\alpha)} > \sqrt{2\cdot(1-\cos(\gamma-\alpha))}$$

and

$$-\sqrt{2\cdot(1-\cos(\gamma+\alpha))} < -\frac{1}{\cos(2\alpha)}\cdot\sqrt{2\cdot(1-\cos(\gamma-\alpha))}$$

are equivalent.

Proof. We start with the first inequality.

$$2\cot(2\alpha)\sqrt{\sin(\gamma)\sin(\alpha)} > \sqrt{2\cdot(1-\cos(\gamma-\alpha))}.$$

We square both sides and divide by two.

$$4\cot^2(2\alpha)\sin(\gamma)\sin(\alpha) > 2\cdot(1-\cos(\gamma-\alpha)).$$

$$2\frac{\cos^2(2\alpha)}{\sin^2(\alpha)}\sin(\gamma)\sin(2\alpha) > 1-\cos(\gamma-\alpha).$$

Because $\cos^2(2\alpha)$ is strictly positive on $0 < \alpha < \frac{\pi}{4}$, we can divide by it.

$$\frac{2\sin(\gamma)\sin(\alpha)}{\sin^2(2\alpha)} > \frac{1-\cos(\gamma-\alpha)}{\cos^2(2\alpha)}.$$

Now, we move both fractions on the same side, combine them into one and use the fact that $2\sin(\gamma)\sin(\alpha) = \cos(\gamma-\alpha)-\cos(\gamma+\alpha)$.

$$\frac{1-\cos(\gamma-\alpha)}{\cos^2(2\alpha)} - \frac{2\sin(\gamma)\sin(\alpha)}{\sin^2(2\alpha)} < 0.$$

$$\frac{(1-\cos(\gamma-\alpha))\cdot\sin^2(2\alpha)-(\cos(\gamma-\alpha)-\cos(\gamma+\alpha))\cdot\cos^2(2\alpha)}{\cos^2(2\alpha)\cdot\sin^2(2\alpha)}<0.$$

We distribute the terms $\sin^2(2\alpha)$ and $\cos^2(2\alpha)$ in the numerator inside the brackets and obtain

$$\frac{\sin^2(2\alpha)-\cos(\gamma-\alpha)+\cos(\gamma+\alpha)\cdot\cos^2(2\alpha)}{\cos^2(2\alpha)\cdot\sin^2(2\alpha)}<0.$$

We add and subtract $\cos^2(2\alpha)$ from the numerator and multiply the inequality by $\sin^2(2\alpha)$, which is also strictly positive on $0<\alpha<\frac{\pi}{4}$.

$$\frac{1-\cos(\gamma-\alpha)+(\cos(\gamma+\alpha)-1)\cdot\cos^2(2\alpha)}{\cos^2(2\alpha)}<0.$$

We split up the fraction again and multiply both sides by two.

$$\frac{2\cdot(1-\cos(\gamma-\alpha))}{\cos^2(2\alpha)}<2\cdot(1-\cos(\gamma+\alpha)).$$

Both sides are positive and hence we can take the square root and finally multiply them by -1.

$$-\frac{1}{\cos(2\alpha)}\sqrt{2\cdot(1-\cos(\gamma-\alpha))}>-\sqrt{2\cdot(1-\cos(\gamma+\alpha))}.$$

This is exactly the second inequality in the statement of the lemma. Crucially, this whole procedure can be done in the other direction as well, and so the claim is proved.

□

Lemma 3.8. Let $\dot{\theta}_n<\omega_b$. Then

$$\dot{\theta}_{n+1}>\dot{\theta}_n.$$

Proof. Clearly,

$$\dot{\theta}_n^2-4\frac{g}{l}\sin(\gamma)\sin(\alpha)<\dot{\theta}_n^2.$$

It follows that

$$\sqrt{\dot{\theta}_n^2-4\frac{g}{l}\sin(\gamma)\sin(\alpha)}<\sqrt{\dot{\theta}_n^2},$$

$$\cos(2\alpha)\sqrt{\dot{\theta}_n^2-4\frac{g}{l}\sin(\gamma)\sin(\alpha)}<|\dot{\theta}_n|,$$

$$-\cos(2\alpha)\sqrt{\dot{\theta}_n^2-4\frac{g}{l}\sin(\gamma)\sin(\alpha)}>-|\dot{\theta}_n|=\dot{\theta}_n,$$

$$\dot{\theta}_{n+1}>\dot{\theta}_n.$$

□

Theorem 3.9. Let $\dot{\theta}_n<\omega_b$. If $\gamma\leq\alpha$, further assume that $\dot{\theta}_n\notin H$. Then $\exists m\in\mathbb{N}$ such that

$$\dot{\theta}_{n+m}>\omega_b.$$

Proof. We will prove this by contradiction. Assume $\dot{\theta}_{n+m} < \omega_b, \quad \forall\, m \in \mathbb{N}$. Then by the Lemma 3.8, the sequence $\dot{\theta}_{n+m}$ is strictly increasing. The only possibility is that it converges to some ω satisfying

$$\omega \leq -\sqrt{2\frac{g}{l}(1-\cos(\gamma+\alpha))}.$$

But from the Lemma 3.1, we have a formula for $\dot{\theta}_{n+m}$. By taking the limit for m going to infinity, we obtain

$$\lim_{m\to\infty}\dot{\theta}_{n+m} = \lim_{m\to\infty}\left(-\cos(2\alpha)\sqrt{\cos^{2(m-1)}(2\alpha)\cdot\dot{\theta}_n^2 - 4\frac{g}{l}\sin(\gamma)\sin(\alpha)\cdot\frac{1-\cos^{2m}(2\alpha)}{1-\cos^2(2\alpha)}}\right)$$

$$\lim_{m\to\infty}\dot{\theta}_{n+m} = -\cos(2\alpha)\sqrt{-4\frac{g}{l}\sin(\gamma)\sin(\alpha)\cdot\frac{1}{1-\cos^2(2\alpha)}}$$

and we have a negative number inside the square root, which is a contradiction with $\dot{\theta}_{n+m}$ converging to ω. Importantly, we were able to take the limit as m goes to infinity only because we assumed that $\dot{\theta}_n \notin H$. Otherwise, the limit would not exist. □

We will use these results later for establishing the exact bounds of the regions of attraction of our fixed points. We start with discussing the stability of ω^*_{stop}.

Theorem 3.10. Let ω^*_{stop} be a fixed point. Then ω^*_{stop} is asymptotically stable for $\gamma < \alpha$ and unstable for $\gamma = \alpha$.

Proof. Assume $\gamma < \alpha$. Let $\varepsilon > 0$. Take $\delta = \min(\varepsilon, \sqrt{2\frac{g}{l}(1-\cos(\gamma-\alpha))})$. Then for any $\dot{\theta}_n$ satisfying

$$|\dot{\theta}_n - \omega^*_{stop}| = |\dot{\theta}_n| < \delta,$$

we have

$$|\dot{\theta}_{n+1} - \omega^*_{stop}| = |\dot{\theta}_{n+1}| = |-\cos(2\alpha)\dot{\theta}_n| = \cos(2\alpha)\cdot|\dot{\theta}_n| < \delta \leq \varepsilon.$$

By induction,

$$|\dot{\theta}_{n+m} - \omega^*_{stop}| < \varepsilon, \qquad \forall m \in \mathbb{N}$$

and thus ω^*_{stop} is stable. Furthermore,

$$\lim_{m\to\infty}|\dot{\theta}_{n+m} - \omega^*_{stop}| = \lim_{m\to\infty}|(-1)^m\cos^m(2\alpha)\dot{\theta}_n| = 0$$

and so it is asymptotically stable as well. Now, in the case of $\gamma = \alpha$, the above proof fails because

$$\min(\varepsilon, \sqrt{2\frac{g}{l}(1-\cos(\gamma-\alpha))}) = 0.$$

For all $\delta > 0$, if $0 < |\dot{\theta}_n| < \delta$, then by the Theorem 3.9, there is some m such that

$$\dot{\theta}_{n+m} > \omega_b$$

and hence

$$\dot{\theta}_{n+m+1} = -\cos(2\alpha)\dot{\theta}_{n+m} > 0.$$

It follows that

$$\dot{\theta}_{n+m+2} = \cos(2\alpha)\sqrt{\dot{\theta}_{n+m+1}^2 + 4\frac{g}{l}\sin(\gamma)\sin(\alpha)}.$$

This means that

$$|\dot{\theta}_{n+m+2}| > \left|\cos(2\alpha)\sqrt{4\frac{g}{l}\sin(\gamma)\sin(\alpha)}\right|,$$

which is a constant. Therefore, if ε is smaller than this constant, it follows that for all $\delta > 0$ and $0 < |\dot{\theta}_n| < \delta$, there is some index m such that $|\dot{\theta}_{n+m+2}| > \varepsilon$ and the proof is done.

□

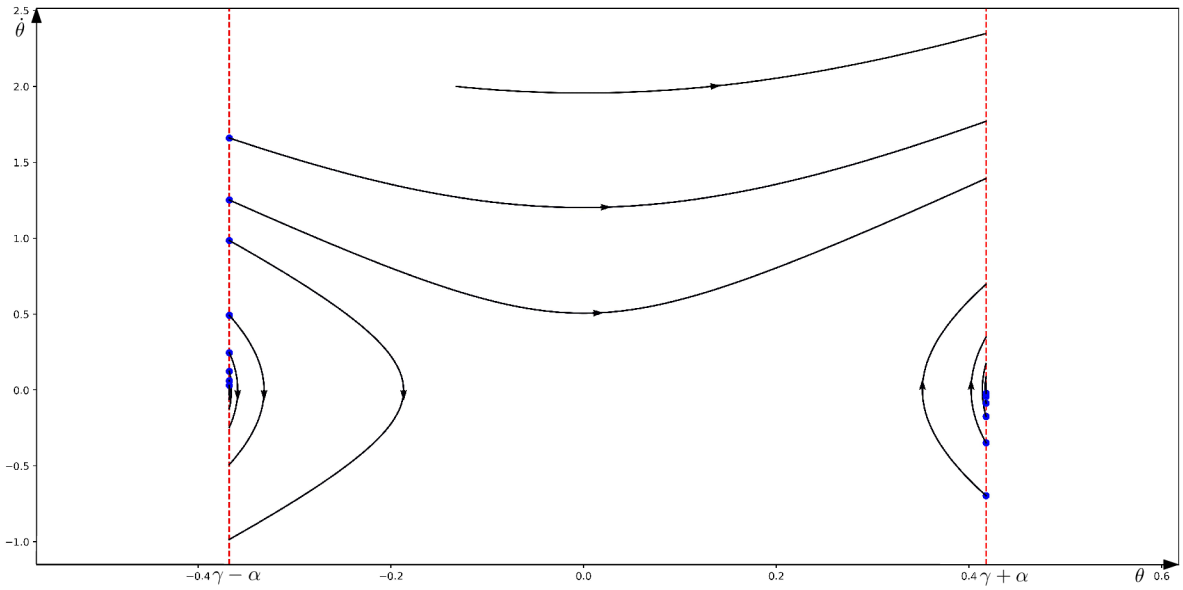

Figure 5. A phase plot of a trajectory with $\dot{\theta}_n$ converging to ω^*_{stop} (with parameters $m = 1, \quad l = 1, \quad g = 9.81, \quad \alpha = \frac{\pi}{8}, \quad \gamma = 0.025$ and initial conditions $\theta(0) = -0.132, \quad \dot{\theta}(0) = 2$).

Before we state the stability theorem of the other fixed point, we first prove two partial results dealing with the monotonicity of the Poincaré map around ω^*_{roll}.

Lemma 3.11. Let $\dot{\theta}_n > \omega^*_{roll}$. Then

$$\omega^*_{roll} < \dot{\theta}_{n+1} < \dot{\theta}_n.$$

Proof. Let $\dot{\theta}_n > \omega^*_{roll}$. Then $\dot{\theta}_n = \omega^*_{roll} + \delta$, where $\delta > 0$.
We first show that $\dot{\theta}_n > \dot{\theta}_{n+1}$. As both of these quantities are non-negative, this is equivalent to showing that $\dot{\theta}_n^2 - \dot{\theta}_{n+1}^2 > 0$. We have

$$\begin{aligned}
\dot{\theta}_n^2 - \dot{\theta}_{n+1}^2 &= (\omega^*_{roll} + \delta)^2 - \cos^2(2\alpha)\left((\omega^*_{roll} + \delta)^2 + 4\frac{g}{l}\sin(\gamma)\sin(\alpha)\right) \\
&= (\omega^*_{roll} + \delta)^2(1 - \cos^2(2\alpha)) - 4\frac{g}{l}\sin(\gamma)\sin(\alpha)\cos^2(2\alpha) \\
&= \sin^2(2\alpha)\left((\omega^*_{roll} + \delta)^2 - 4\cot^2(2\alpha)\frac{g}{l}\sin(\gamma)\sin(\alpha)\right) \\
&= \sin^2(2\alpha)\left((\omega^*_{roll} + \delta)^2 - \omega^{*2}_{roll}\right) = \sin^2(2\alpha)(2\omega^*_{roll}\delta + \delta^2) > 0.
\end{aligned}$$

For the second part of our proposition, namely $\dot{\theta}_{n+1} > \omega^*_{roll}$, it is sufficient to observe that

$$\begin{aligned}\dot{\theta}^2_{n+1} - \omega^{*2}_{roll} &= \dot{\theta}^2_{n+1} - \dot{\theta}^2_n + \dot{\theta}^2_n - \omega^{*2}_{roll} \\ &= -\sin^2(2\alpha)(2\omega^*_{roll}\delta + \delta^2) + (\omega^*_{roll} + \delta)^2 - \omega^{*2}_{roll} \\ &= -\sin^2(2\alpha)(2\omega^*_{roll}\delta + \delta^2) + 2\omega^*_{roll}\delta + \delta^2 \\ &= \cos^2(2\alpha)(2\omega^*_{roll}\delta + \delta^2) > 0.\end{aligned}$$

□

Lemma 3.12. Let $\omega_f < \dot{\theta}_n < \omega^*_{roll}$. Then

$$\dot{\theta}_n < \dot{\theta}_{n+1} < \omega^*_{roll}.$$

Proof. Let $\omega_f < \dot{\theta}_n < \omega^*_{roll}$.
Then $\dot{\theta}_n = \omega^*_{roll} - \delta$, where $0 < \delta < \omega^*_{roll} - \sqrt{2\frac{g}{l}(1 - \cos(\gamma - \alpha))}$. In the exact same way as in the proof of Lemma 3.11, we end up with

$$\dot{\theta}^2_{n+1} - \dot{\theta}^2_n = -\sin^2(2\alpha)(-2\omega^*_{roll}\delta + \delta^2),$$

and because of our conditions on δ, we also have

$$\delta < 2\omega^*_{roll},$$

$$-2\omega^*_{roll}\delta + \delta^2 < 0.$$

This gives us the inequality $\dot{\theta}_{n+1} > \dot{\theta}_n$.
For the other one, we again have

$$\begin{aligned}\omega^{*2}_{roll} - \dot{\theta}^2_{n+1} &= \omega^{*2}_{roll} - \dot{\theta}^2_{n+1} + \dot{\theta}^2_n - \dot{\theta}^2_n \\ &= -\cos^2(2\alpha)(-2\omega^*_{roll}\delta + \delta^2) > 0.\end{aligned}$$

□

Remark. For $\gamma > \alpha$, the assumptions on $\dot{\theta}_n$ in Lemma 3.12 can be relaxed into

$$0 \leq \dot{\theta}_n < \omega^*_{roll}.$$

This is possible because of a different definition of the Poincaré map for $\gamma > \alpha$ (see (3.14)).

At this point, we can procede to state and prove the stability theorem of ω^*_{roll}.

Theorem 3.13. Let ω^*_{roll} be a fixed point. Then ω^*_{roll} is asymptotically stable.

Proof. Let $\varepsilon > 0$. Take $\delta = \min(\varepsilon, \omega^*_{roll} - \sqrt{2\frac{g}{l}(1 - \cos(\gamma - \alpha))})$. Then for any $\dot{\theta}_n$ satisfying

$$\left|\dot{\theta}_n - \omega^*_{roll}\right| < \delta,$$

as a corollary of Lemma 3.11 and Lemma 3.12, we have

$$\left|\dot{\theta}_{n+1} - \omega^*_{roll}\right| < \left|\dot{\theta}_n - \omega^*_{roll}\right| < \delta \leq \epsilon.$$

By induction,

$$\left|\dot{\theta}_{n+m} - \omega^*_{roll}\right| < \varepsilon, \quad \forall m \in \mathbb{N}$$

and thus ω^*_{roll} is stable.
Furthermore, thanks to the combination of Lemma 3.11 and Lemma 3.12, it follows that if

$$\dot{\theta}_n > \omega_f,$$

then $\forall m \in \mathbb{N}$,

$$\dot{\theta}_{n+m} > \omega_f.$$

This makes it possible for us to evaluate the following limit.

$$\begin{aligned}
&\lim_{m\to\infty}\left|\dot{\theta}_{n+m} - \omega^*_{roll}\right| = \left|\lim_{m\to\infty}\left(\dot{\theta}_{n+m}\right) - \omega^*_{roll}\right| \\
&= \left|\lim_{m\to\infty}\left(\cos(2\alpha)\sqrt{\cos^{2(m-1)}(2\alpha)\cdot\dot{\theta}_n^2 + 4\frac{g}{l}\sin(\gamma)\sin(\alpha)\cdot\frac{1-\cos^{2m}(2\alpha)}{1-\cos^2(2\alpha)}}\right) - \omega^*_{roll}\right| \\
&= \left|\cos(2\alpha)\sqrt{4\frac{g}{l}\sin(\gamma)\sin(\alpha)\cdot\frac{1}{\sin^2(2\alpha)}} - \omega^*_{roll}\right| \\
&= \left|2\cot(2\alpha)\sqrt{\frac{g}{l}\sin(\gamma)\sin(\alpha)} - \omega^*_{roll}\right| = \left|\omega^*_{roll} - \omega^*_{roll}\right| = 0.
\end{aligned}$$

□

It remains to find the exact bounds of regions of attraction for both fixed points.

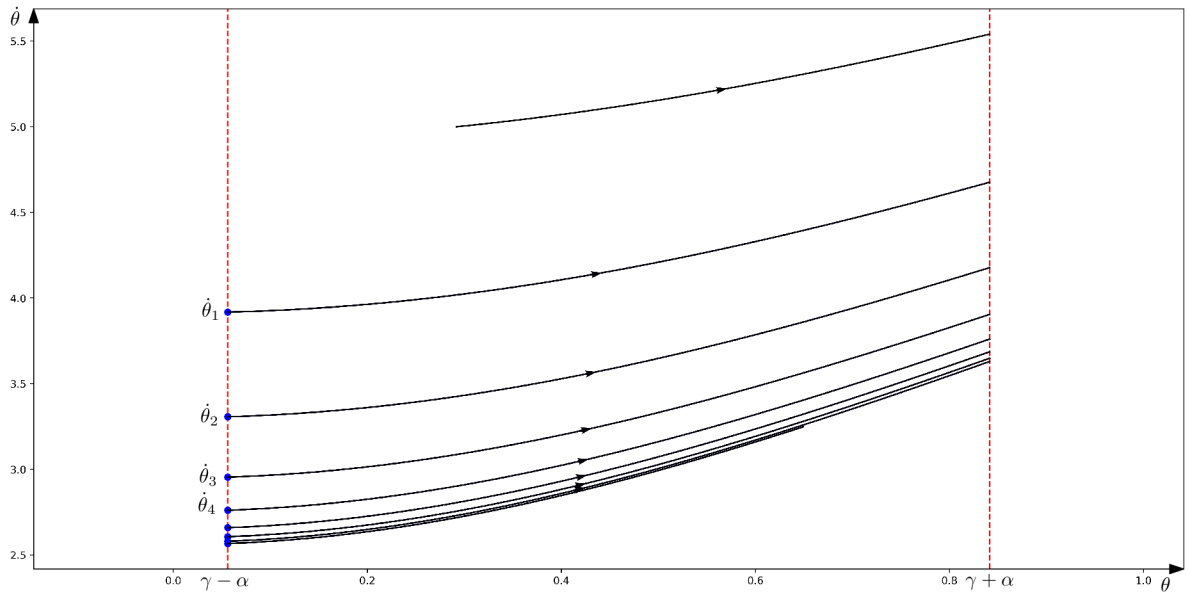

Figure 6. A phase plot of a trajectory with $\dot{\theta}_n$ converging to ω^*_{roll} from above (with parameters $m = 1, \quad l = 1, \quad g = 9.81, \quad \alpha = \frac{\pi}{8}, \quad \gamma = \frac{\pi}{7}$ and initial conditions $\theta(0) = 0.292, \quad \dot{\theta}(0) = 5$).

3.3.5 Regions of Attraction

Because of the dependence on parameters γ and α, we divide our discussion of the fixed points' regions of attraction into five distinct cases covering the whole region $\Omega_{(\alpha,\gamma)}$ of admissible angles α and γ defined in (3.1). We define these cases followingly.

$$\Omega_1 = \{(\alpha,\gamma) \in \Omega_{(\alpha,\gamma)} \mid \quad \gamma > \alpha\}.$$

$$\Omega_2 = \{(\alpha,\gamma) \in \Omega_{(\alpha,\gamma)} \mid \quad \gamma = \alpha\}.$$

$$\Omega_3 = \{(\alpha,\gamma) \in \Omega_{(\alpha,\gamma)} \mid \gamma < \alpha,\ 2\cot(2\alpha)\sqrt{\sin(\gamma)\sin(\alpha)} < \sqrt{2(1-\cos(\gamma-\alpha))}\}.$$

$$\Omega_4 = \{(\alpha,\gamma) \in \Omega_{(\alpha,\gamma)} \mid \gamma < \alpha,\ 2\cot(2\alpha)\sqrt{\sin(\gamma)\sin(\alpha)} = \sqrt{2(1-\cos(\gamma-\alpha))}\}.$$

$$\Omega_5 = \{(\alpha,\gamma) \in \Omega_{(\alpha,\gamma)} \mid \gamma < \alpha,\ 2\cot(2\alpha)\sqrt{\sin(\gamma)\sin(\alpha)} > \sqrt{2(1-\cos(\gamma-\alpha))}\}.$$

Clearly,

$$\bigcup_{i=1}^{5} \Omega_i = \Omega_{(\alpha,\gamma)}$$

We will denote the two fixed points' regions of attraction by $R_A(\omega^*_{stop})$ and $R_A(\omega^*_{roll})$.

We begin with the most straightforward case, which is that of $(\alpha,\gamma) \in \Omega_1$. As it was shown and explained earlier in the chapter concerning the existence of fixed points, in the event of $\gamma > \alpha$, the fixed point ω^*_{stop} vanishes. On the other hand, the condition $\gamma > \alpha$ is sufficient for the presence of ω^*_{roll}.

Theorem 3.14. Let $(\alpha,\gamma) \in \Omega_1$. Then ω^*_{roll} is an asymptotically stable fixed point with a region of attraction

$$R_A(\omega^*_{roll}) = \mathbb{R}.$$

Proof. For $\gamma > \alpha$, the fixed point ω^*_{roll} always exists and by Theorem 3.13, it is asymptotically stable. From the choice of δ in the proof of the Theorem 3.13, we immediately get a first estimate for the region of attraction.

$$R_A(\omega^*_{roll}) \supseteq (\omega_f, \infty).$$

The left bound is of this form to allow the use of Lemma 3.12 in the proof. However, as was noted earlier, in the case of $\gamma > \alpha$ the assumptions of Lemma 3.12 can be relaxed. This gives us a new estimate

$$R_A(\omega^*_{roll}) \supseteq [0, \infty).$$

Continuing in the same fashion, we can extend this to include $(\omega_b, 0)$ as well. This is justified because if

$$\dot{\theta}_n \in (\omega_b, 0),$$

then

$$\dot{\theta}_{n+1} = -\cos(2\alpha)\dot{\theta}_n$$

and so $\dot{\theta}_{n+1} > 0$. That implies that $\dot{\theta}_{n+1} \in R_A(\omega^*_{roll})$ and hence $\dot{\theta}_n \in R_A(\omega^*_{roll})$. This gives us

$$R_A(\omega^*_{roll}) \supseteq (\omega_b, \infty).$$

Finally, the Theorem 3.9 says that if $\dot{\theta}_n \leq \omega_b$, then there exists some m such that

$$\dot{\theta}_{n+m} > \omega_b$$

and so $\dot{\theta}_{n+m} \in R_A(\omega^*_{roll})$. This implies that $\dot{\theta}_n \in R_A(\omega^*_{roll})$. It follows that

$$R_A(\omega^*_{roll}) = (-\infty, \infty)$$

and the proof is done. □

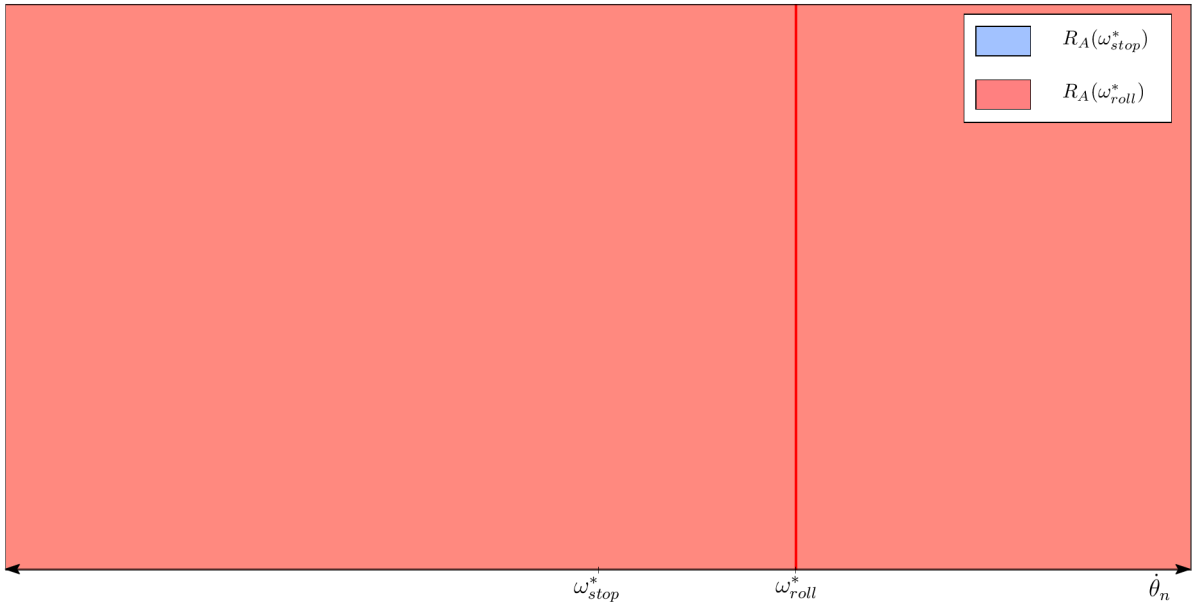

Figure 7. Stability plot with $(\alpha, \gamma) \in \Omega_1$.

Next, we investigate Ω_2. From previous analysis, we know that the fixed point ω^*_{stop} exists and it is unstable. We can also see that the by plugging in $\gamma = \alpha$, the condition (3.16) for existence of ω^*_{roll}

$$2\cot(2\alpha)\sqrt{\sin(\gamma)\sin(\alpha)} > \sqrt{2(1-\cos(\gamma-\alpha))}$$

reduces to the simple

$$\cot(2\alpha) \cdot |\sin(\alpha)| > 0,$$

which is satisfied for all $\alpha \in (0, \frac{\pi}{4})$.

Theorem 3.15. Let $(\alpha, \gamma) \in \Omega_2$. Then ω^*_{stop} is an unstable fixed point and ω^*_{roll} is an asymptotically stable fixed point with a region of attraction

$$R_A(\omega^*_{roll}) = \mathbb{R} \setminus (\{0\} \cup H).$$

Proof. The idea of the proof is identical to that of Theorem 3.14. The only change is that we cannot relax our assumptions on Lemma 3.12. That particular step in the proof then yields a weaker estimate

$$R_A(\omega^*_{roll}) \supseteq (0, \infty),$$

with zero excluded from the interval. The remaining extension to the interval $(-\infty, 0)$ is unchanged. Of course, we cannot include the sets H_1 and H_2 in the region of attraction because in that case the limit $\lim_{m\to\infty}(\dot{\theta}_{n+m})$ would not exist. □

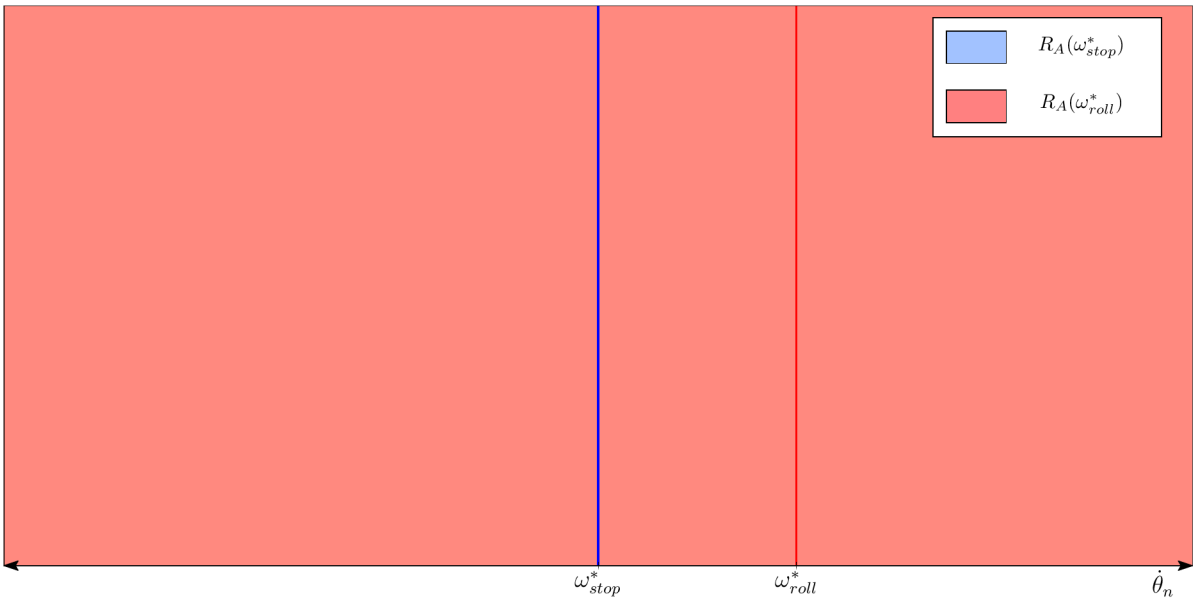

Figure 8. Stability plot with $(\alpha, \gamma) \in \Omega_2$.

The third possibility is that $(\alpha, \gamma) \in \Omega_3$. This means that the Poincaré map has only one fixed point, ω^*_{stop}. Before we find its region of attraction, we prove a helpful lemma.

Lemma 3.16. Let $(\alpha, \gamma) \in \Omega_3$. Let $\dot{\theta}_n > \omega_f$, $\dot{\theta}_n \notin H$.
Then $\exists m \in \mathbb{N}$ such that $\dot{\theta}_{n+m} < \omega_f$.

Proof. We prove this by contradiction. Let $\dot{\theta}_{n+i} \geq \omega_f$ for all $i \in \mathbb{N}$. Then by our assumption,

$$\dot{\theta}_{n+i} > 2\cot(2\alpha)\sqrt{\frac{g}{l}\sin(\gamma)\sin(\alpha)}$$

and so by Lemma 3.4,

$$\dot{\theta}_{n+i} = \cos(2\alpha)\sqrt{\cos^{2(i-1)}(2\alpha)\cdot\dot{\theta}_n^2 + 4\frac{g}{l}\sin(\gamma)\sin(\alpha)\cdot\frac{1-\cos^{2i}(2\alpha)}{1-\cos^2(2\alpha)}}, \quad \forall i \in \mathbb{N}.$$

But as was shown in the proof of Theorem 3.13, this sequence converges to $2\cot(2\alpha)\sqrt{\frac{g}{l}\sin(\gamma)\sin(\alpha)}$, which is a contradiction with the assumption that

$$2\cot(2\alpha)\sqrt{\sin(\gamma)\sin(\alpha)} < \sqrt{2(1-\cos(\gamma-\alpha))}.$$

□

Theorem 3.17. Let $(\alpha, \gamma) \in \Omega_3$. Then ω^*_{stop} is an asymptotically stable fixed point with a region of attraction

$$R_A(\omega^*_{stop}) = \mathbb{R} \setminus H.$$

Proof. From $\gamma < \alpha$, we know that the fixed point ω^*_{stop} exists and by Theorem 3.10, it is asymptotically stable. On the other hand,

$$2\cot(2\alpha)\sqrt{\sin(\gamma)\sin(\alpha)} < \sqrt{2(1-\cos(\gamma-\alpha))}$$

implies that the fixed point ω^*_{roll} does not exist.
From the proof of Theorem 3.10, we immediately obtain an initial estimate

$$R_A(\omega^*_{stop}) \supseteq (-\omega_f, \omega_f)\,.$$

Lemma 3.16 then provides a clear way to extend the region to the interval

$$(\omega_f, \infty) \setminus H.$$

Let $\dot{\theta}_n$ lie inside this set. Then by Lemma 3.16, there exists an $m \in \mathbb{N}$ such that $\dot{\theta}_{n+m} < \omega_f$, and so

$$\dot{\theta}_{n+m} \in R_A(\omega^*_{stop}),$$

which implies

$$\dot{\theta}_n \in R_A(\omega^*_{stop}).$$

It is simple to verify that if $\dot{\theta}_n \in \left(-\frac{1}{\cos(2\alpha)} \cdot \omega_f, -\omega_f\right)$, then

$$\dot{\theta}_{n+1} \in (0, \omega_f)$$

and thus we can extend $R_A(\omega^*_{stop})$ to

$$\left(-\frac{1}{\cos(2\alpha)} \cdot \omega_f, \infty\right) \setminus H$$

Thanks to Lemma 3.7, we know that

$$(\omega_b, 0) \subset R_A(\omega^*_{stop}),$$

and by using Theorem 3.9 in the same way as Lemma 3.16, we can extend this to $(-\infty, \omega_b)$, too. □

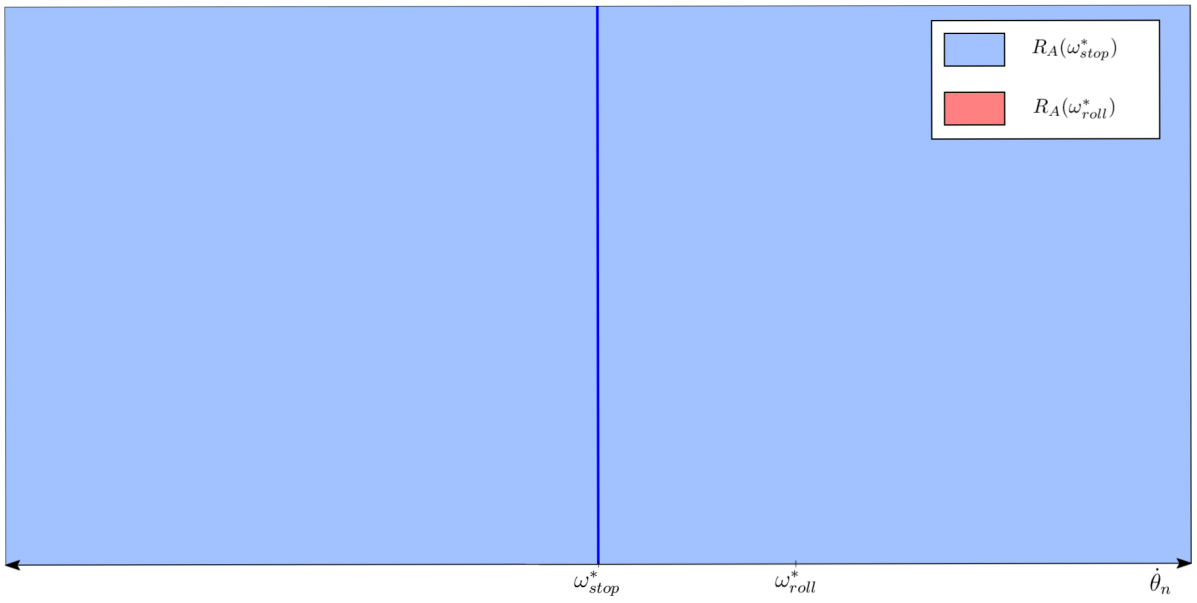

Figure 9. Stability plot with $(\alpha, \gamma) \in \Omega_3$.

The fourth option is that $(\alpha, \gamma) \in \Omega_4$. We still only have the fixed point ω^*_{stop}. The other fixed point ω^*_{roll} does not exist, but in a sense it is asymptotically stable from above, as we show below.

Lemma 3.18. Let $(\alpha, \gamma) \in \Omega_4$. Let $\dot{\theta}_n > \omega_f$, $\dot{\theta}_n \notin H$.
Then

$$\lim_{m\to\infty} \dot{\theta}_{n+m} = \omega^*_{roll}.$$

Proof. This follows from the combination of Lemma 3.4 and Lemma 3.11. □

Theorem 3.19. Let $(\alpha, \gamma) \in \Omega_4$. Then ω^*_{stop} is an asymptotically stable fixed point with a region of attraction

$$R_A(\omega^*_{stop}) = (-\infty, \omega_f) \setminus H.$$

Proof. The proof is identical to that of Theorem 3.17, with the difference that it is not possible to use Lemma 3.16 to extend $R_A(\omega^*_{stop})$ above the value $\sqrt{2\frac{g}{l}(1-\cos(\gamma-\alpha))}$. In fact, Lemma 3.18 shows that values from the interval $\left(\sqrt{2\frac{g}{l}(1-\cos(\gamma-\alpha))}, \infty\right)$ converge to $\sqrt{2\frac{g}{l}(1-\cos(\gamma-\alpha))}$. □

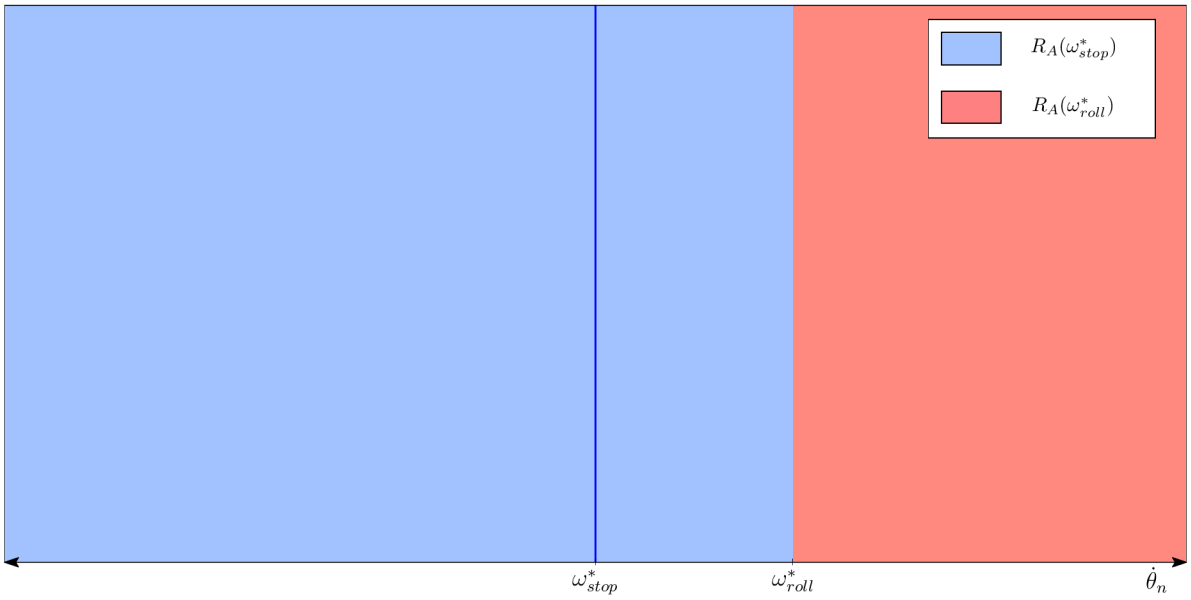

Figure 10. Stability plot with $(\alpha, \gamma) \in \Omega_4$.

Remark. Although the fixed point ω^*_{roll} does not exist, we can see that the point $2\cot(2\alpha)\sqrt{\frac{g}{l}\sin(\gamma)\sin(\alpha)}$ is semistable from above.

Finally, we move to the last possibility, namely that $(\alpha, \gamma) \in \Omega_5$. This is by far the most interesting one, as both fixed points exist and have their own regions of attraction. Before we state the theorem, we introduce the following notation.

Definition 3.20. Let $(\alpha, \gamma) \in \Omega_5$. Let

$$\omega_1^0 = \omega_b,$$

$$\omega_2^0 = -\frac{1}{\cos(2\alpha)}\omega_f.$$

Let $m \in \mathbb{N}$. By ω_1^m and ω_2^m we denote the values from the interval $(-\infty, \omega_2^0)$ satisfying

$$\omega_1^m = \dot{\theta}_{n-m}, \quad \text{where } \dot{\theta}_n = \omega_1^0,$$

$$\omega_2^m = \dot{\theta}_{n-m}, \quad \text{where } \dot{\theta}_n = \omega_2^0.$$

Then we define the sets I_{roll}^m and I_{stop}^m as

$$I_{roll}^m = \left(\omega_1^m, \omega_2^m\right),$$

$$I_{stop}^m = \left(\omega_2^{m+1}, \omega_1^m\right).$$

It is important to note that the validity of this definition comes from Lemma 3.7. Otherwise we could not have known whether $\omega_1^0 < \omega_2^0$ was actually true.

Remark. Lemma 3.2 gives us closed formulas for ω_1^m and ω_2^m.

$$\omega_1^m = -\sqrt{2\frac{g}{l} \cdot \left(\cos^{-2m}(2\alpha) \cdot (1 - \cos(\gamma + \alpha)) + 2\sin(\gamma)\sin(\alpha) \cdot \frac{1 - \cos^{-2m}(2\alpha)}{1 - \cos^{-2}(2\alpha)}\right)}.$$

$$\omega_2^m = -\sqrt{2\frac{g}{l} \cdot \left(\cos^{-2(m+1)}(2\alpha) \cdot (1 - \cos(\gamma - \alpha)) + 2\sin(\gamma)\sin(\alpha) \cdot \frac{1 - \cos^{-2m}(2\alpha)}{1 - \cos^{-2}(2\alpha)}\right)}.$$

Remark. The elements of H_1 and H_2 form the boundary of the union of all I_{roll}^m and I_{stop}^m. In other words,

$$(-\infty, \omega_2^0) \subset \left(\left(\bigcup_{m=0}^{\infty} I_{roll}^m \cup I_{stop}^m\right) \cup H\right).$$

We are prepared to state the theorem itself.

Theorem 3.21. Let $(\alpha, \gamma) \in \Omega_5$. Then ω_{stop}^* is an asymptotically stable fixed point with a region of attraction

$$R_A(\omega_{stop}^*) = \left(\left(\omega_2^0, \omega_f\right) \cup \left(\bigcup_{m=0}^{\infty} I_{stop}^m\right)\right) \setminus H \tag{3.17}$$

and ω_{roll}^* is an asymptotically stable fixed point with a region of attraction

$$R_A(\omega_{roll}^*) = \left((\omega_f, \infty) \cup \left(\bigcup_{m=0}^{\infty} I_{roll}^m\right)\right) \setminus H. \tag{3.18}$$

Proof. The conditions for the existence of both fixed points are satisfied and from Theorems 3.10 and 3.13, we know that they are both asymptotically stable. From the proofs of these theorem, we immediately obtain first estimates for their regions of attraction.

$$R_A(\omega_{stop}^*) \supseteq (-\omega_f, \omega_f),$$

$$R_A(\omega_{roll}^*) \supseteq (\omega_f, \infty).$$

As a consequence of Lemma 3.7, we know that

$$\omega_1^0 < \omega_2^0 < -\omega_f,$$

where ω_1^0 and ω_2^0 are defined according to Definition 3.20. It is straightforward to see that if

$$\dot{\theta}_n \in \left(\omega_2^0, -\omega_f\right),$$

then

$$\dot{\theta}_{n+1} = -\cos(2\alpha) \cdot \dot{\theta}_n \in (\cos(2\alpha) \cdot \omega_f, \omega_f),$$

and hence $\dot{\theta}_{n+1} \in R_A(\omega^*_{stop})$, which implies

$$\dot{\theta}_n \in R_A(\omega^*_{stop}).$$

On the other hand, if

$$\dot{\theta}_n \in \left(\omega_1^0, \omega_2^0\right),$$

then

$$\dot{\theta}_{n+1} = -\cos(2\alpha) \cdot \dot{\theta}_n \in \left(\omega_f, -\cos(2\alpha) \cdot \omega_1^0\right).$$

by the same logic as before,

$$\dot{\theta}_n \in R_A(\omega^*_{roll}).$$

To extend the regions to $-\infty$, we simply use the intervals I^m_{stop} and I^m_{roll} from Definition 3.20. Thanks to the continuity of the Poincaré map, if $\dot{\theta}_n \in I^m_{stop}$, then

$$\dot{\theta}_{n+m} \in \left(\omega_2^0, -\omega_f\right),$$

and if $\dot{\theta}_n \in I^m_{roll}$, then

$$\dot{\theta}_{n+m} \in \left(\omega_1^0, \omega_2^0\right).$$

This completes the proof. □

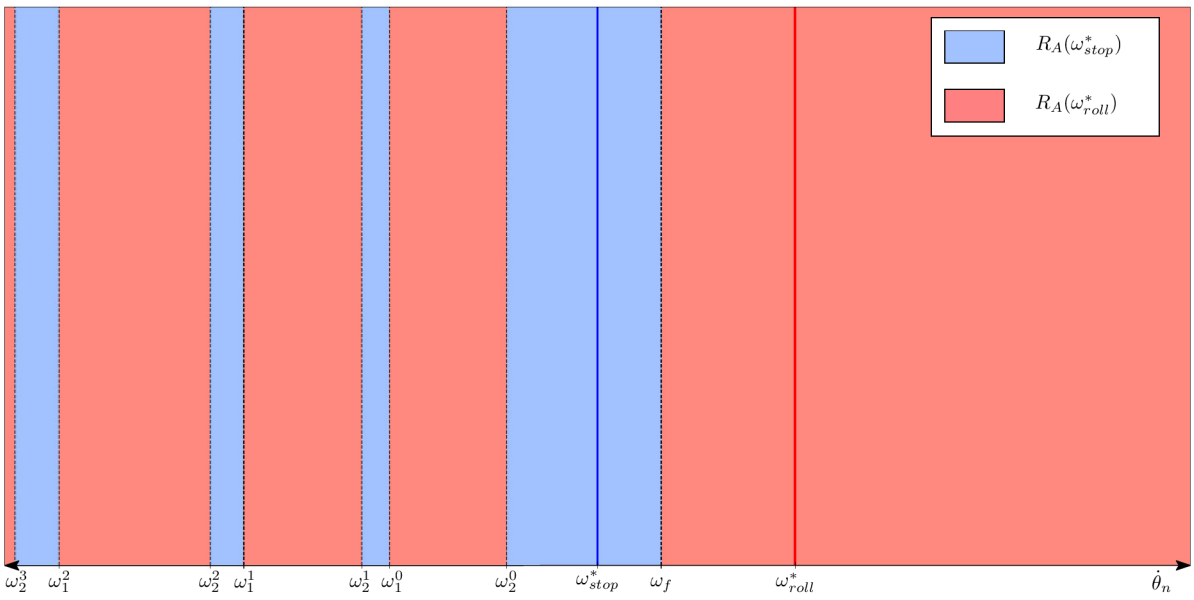

Figure 11. Stability plot with $(\alpha, \gamma) \in \Omega_5$.

To better see how this works in action, we include phase plots of two trajectories with identical model parameters satisfying $(\alpha, \gamma) \in \Omega_5$ (see Figures 12 and 13). They only differ slightly in their initial value of $\dot{\theta}$. In the first case, $\dot{\theta}(0) = -5$ lies in one of the intervals I^m_{roll}, while for the second trajectory, $\dot{\theta}(0) = -4.85$ belongs to one of I^m_{stop}. This has the consequence that their long-term behaviors are in total contrast.

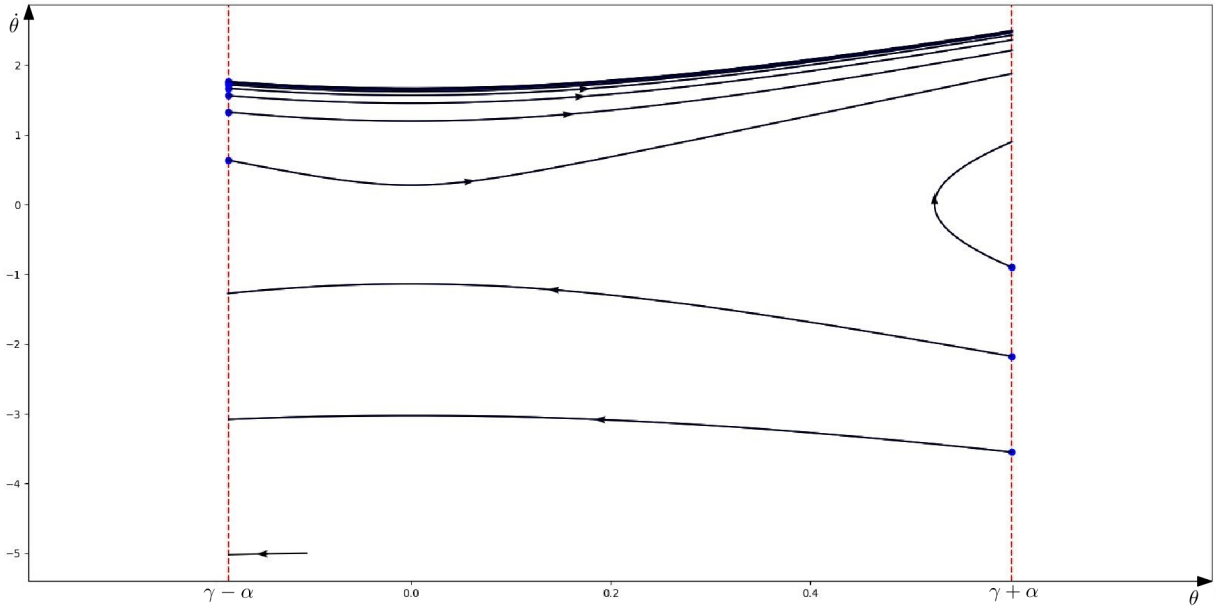

Figure 12. A phase plot of a trajectory with $\dot{\theta}_n$ converging to ω^*_{roll} from below (with parameters $m = 1, \quad l = 1, \quad g = 9.81, \quad \alpha = \frac{\pi}{8}, \quad \gamma = \frac{\pi}{15}$ and initial conditions $\theta(0) = -0.105, \quad \dot{\theta}(0) = -5$).

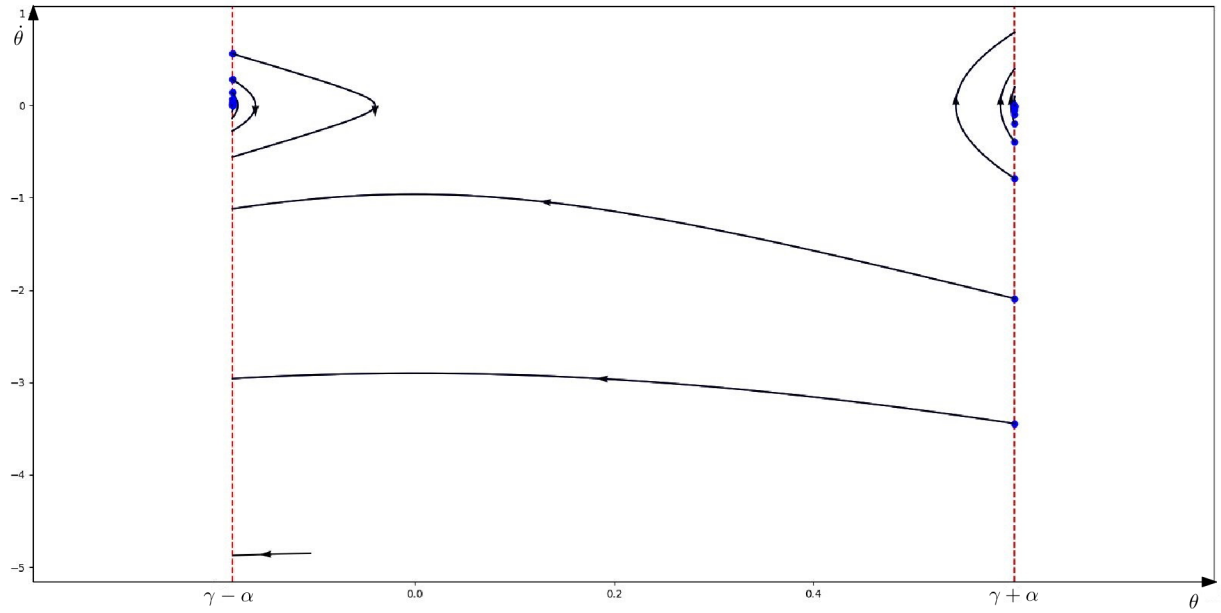

Figure 13. A phase plot of a trajectory with $\dot{\theta}_n$ converging to ω^*_{stop} (with parameters $m = 1, \quad l = 1, \quad g = 9.81, \quad \alpha = \frac{\pi}{8}, \quad \gamma = \frac{\pi}{15}$ and initial conditions $\theta(0) = -0.105, \quad \dot{\theta}(0) = -4.85$).

3.4 Summary

To conclude the section about the rimless wheel model, we summarize the results of our analysis and accompany them with their graphical representation. First, we derived the differential equation governing the wheel's motion between each two collisions. Then, we found a relationship of the wheel's state right before and right after a collision, based on the law of conversation of angular momentum. We merged these to define a Poincaré map, which we then used to find out what happens in the long term. Most of our work was concerned with analysing the stability and finding the regions of attraction of the map's fixed points.
The result is that given arbitrary initial conditions (angle θ and angular velocity $\dot{\theta}$), one can solve the differential equation (3.2) and apply the collision factor $\cos(2\alpha)$ to find the initial value $\dot{\theta}_0$ for the Poincaré map. Depending on the relationship between the parameters α and γ, it is possible to say exactly to which long-term behavior it converges. The long-term behavior is summarized in Table 1.
To better convey the nature of the sets Ω_i partitioning $\Omega_{(\alpha,\gamma)}$, we visualize them in Fig. 14.

As a closing remark, we come back to the very beginning of the section where we introduced natural assumptions on the parameters of the model, namely that $\gamma > 0$. Indeed, this premise was unnecessary as we could also allow γ to be equal to zero. In that case, we would obtain symmetry between the forward and backward motion regimes and the wheel would not be able to ever increase its total energy.
We could then introduce the Poincaré map in the same way as in (3.13), and after doing stability analysis, we would arrive at the conclusion that the case $\gamma = 0$ can be described by the results derived for the region Ω_3.

	Ω_1	Ω_2	Ω_3	Ω_4	Ω_5
Existence of ω^*_{stop}	✗	✓	✓	✓	✓
Existence of ω^*_{roll}	✓	✓	✗	✗	✓
Stability of ω^*_{stop}	—	unstable	as. stable	as. stable	as. stable
Stability of ω^*_{roll}	as. stable	as. stable	—	—	as. stable
$R_A(\omega^*_{stop})$	—	$\{0\}$	$\mathbb{R} \setminus H$	$(-\infty, \omega_f) \setminus H$	see (3.17)
$R_A(\omega^*_{roll})$	$\mathbb{R}$	$\mathbb{R} \setminus \{0\}$	—	$(\omega_f, \infty) \setminus H$	see (3.18)
Stability plot	Fig. 7	Fig. 8	Fig. 9	Fig. 10	Fig. 11

Table 1: Summary of the Poincaré map's fixed points' existence and stability for different configurations of α and γ. For the purposes of compactness, the regions of attraction for Ω_5 are only referred to by their equation numbers.

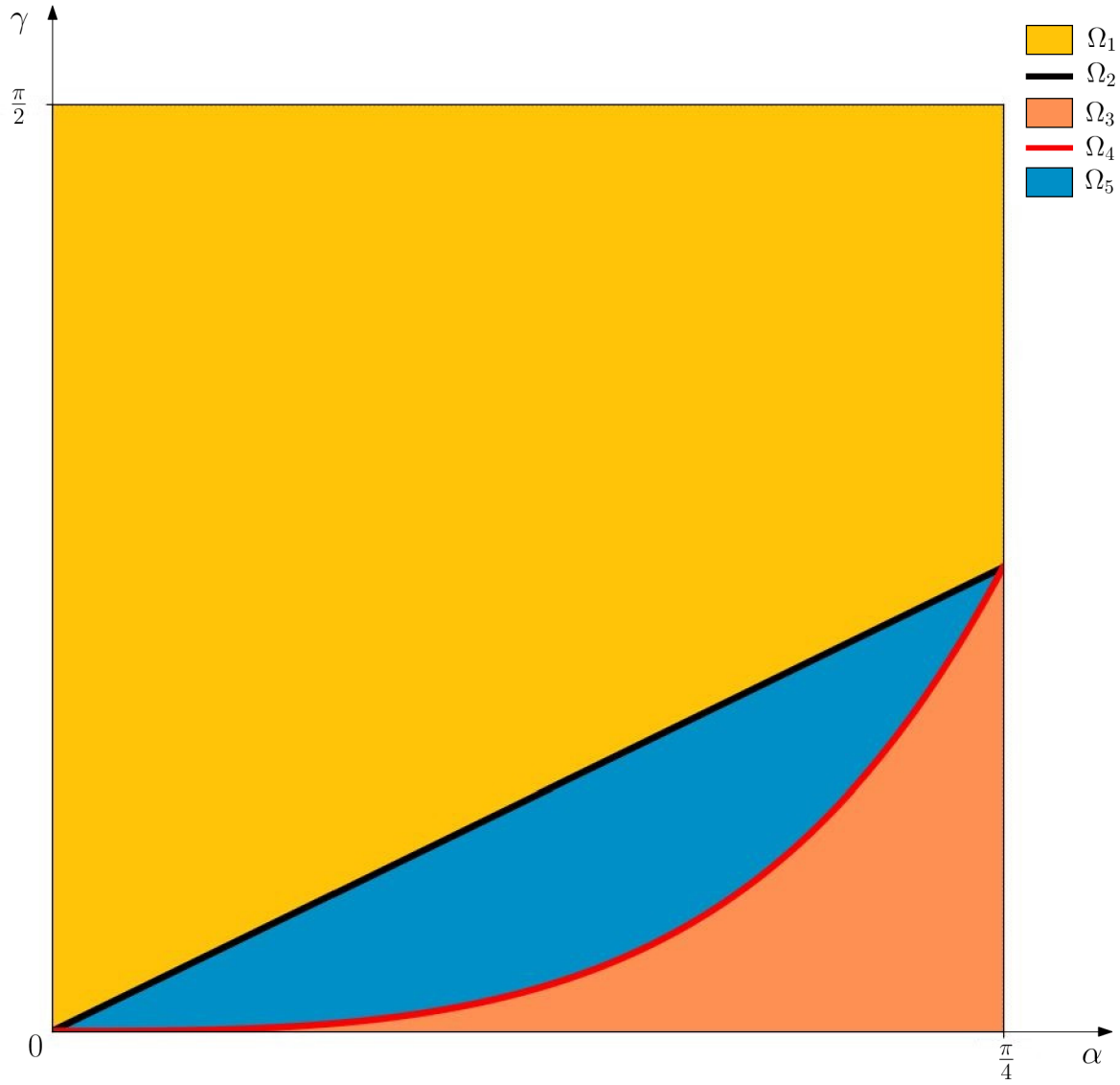

Figure 14. The region of admissible angles α and γ divided into Ω_i as defined in Subsection 3.3.5.

4 The Compass Gait Biped

The second model that we are going to introduce and study is the *compass gait biped*, also known as *2-link* or *acrobot*. In a way, it arises naturally from the rimless wheel, which models the dynamics of the stance leg and always has another leg ready to take over at impact. This is of course accomplished by the wheel's rigid frame with spokes evenly spaced around its center of mass.
We can imagine getting rid of all but two of the wheel's legs and introducing a way for the swing leg to position itself to collide with the ground and successfully make a step. This change complicates the matter greatly because then the robot is no longer passive. It requires active control to ensure that it walks.
The control is accomplished by adding an actuator to the robot's "hip" (the place where the two legs are joined). The actuator can then supply torque to the system and thus manage its behavior. Of course, even after adding the actuator, the robot is still underactuated because it has two degrees of freedom. This is so because in contrast with the rimless wheel, where knowing the angle θ between the stance leg and a vertical line was enough to exactly identify the state of the system, in the case of the compass gait biped, the angle between the stance leg and the swing leg changes dynamically. In view of this, we must make use of the underlying dynamics of the system to successfully guide the biped's walk.

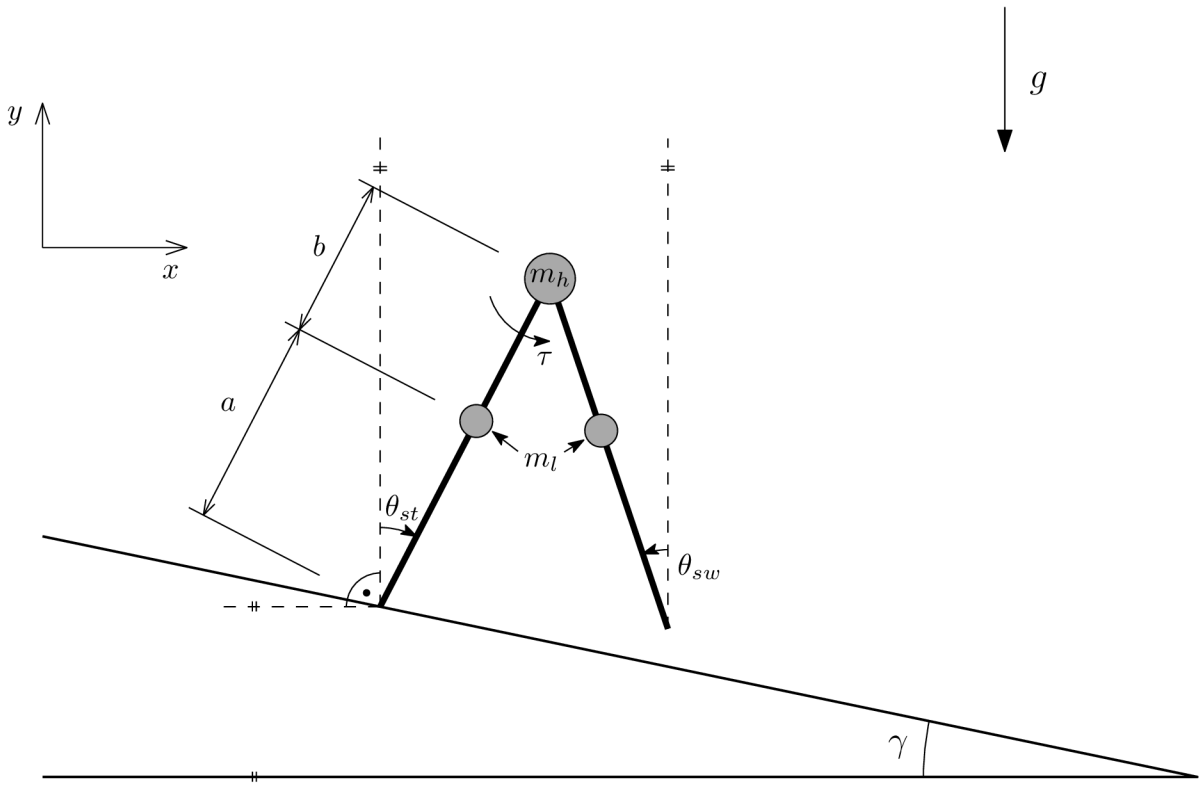

Figure 15. The compass gait biped model.

As a consequence of adding external torque to the biped's hip, we must get rid of our assumption that the legs are massless. This is represented by adding point masses to both legs.

The modelling assumptions are esentially the same as in the rimless wheel model. We briefly summarize them here.

- The legs are rigid bodies, all of their masses are concentrated in a point.
- The legs' collisions with the ground are perfectly inelastic and impulsive.
- The collisions are instantenous.
- The legs cannot slip.
- The swing leg retracts a little without changing the location of its point mass.

The last assumption is a bit unnatural, but it is necessary for the model to work. Consider that when the swing leg moves from left to right to position itself for impact, it must inevitably pass around the stance leg. However, as they have the same length, this would lead to the swing leg's hitting the ground and stumbling. Our premise that after a collision the swing leg retracts a little bit solves this issue.
We will also require the hip and the swing leg's endpoint to stay above the ground. We will deal with the statement of this requirement after we solve the kinematics in the swing phase model subsection.
The system is fully specified by five parameters. These are γ, the angle of the ramp's slope, m_h, the mass located at the hip, m_l, which specifies the leg masses, and lengths a and b determining the exact position of the leg masses. By $l = a + b$, we will denote the legs' length. Fig. 15 shows this in detail.
We have some natural assumptions on these parameters.

$$0 \leq \gamma < \frac{\pi}{2}, \qquad a > 0, \qquad b > 0, \qquad g > 0, \qquad m_h > 0, \qquad m_l > 0.$$

The angles θ_{st} and θ_{sw} corresponding to the stance leg and the swing leg are directed angles with the positive direction being the clockwise one, just like in the rimless wheel case.
The torque of the actuator at the hip is represented by τ. Its positive direction is counterlockwise as shown in Fig. 15.

The initial procedure in analysing the compass gait biped is identical. We must first deal with the swing phase, studying the system's kinematics and dynamics. Then, we will look at what happens when the swing leg impacts the ground.

4.1 Swing Phase Model

The robot's configuration is described by the two angles θ_{st} and θ_{sw} which form the vector of generalized coordinates

$$\mathbf{q}(t) = \begin{bmatrix} \theta_{st}(t) \\ \theta_{sw}(t) \end{bmatrix}.$$

We place the origin of the Cartesian coordinate system to the endpoint of the stance leg. We denote by $\mathbf{x}_{st}$ the position of m_{st}, by $\mathbf{x}_h$ the position of m_h, by $\mathbf{x}_{sw}$ the position of m_{sw} and by $\mathbf{x}_e$ the position of the endpoint of the swing leg. Similarly, by $\dot{\mathbf{x}}_{st}$, $\dot{\mathbf{x}}_h$, $\dot{\mathbf{x}}_{sw}$,

and $\dot{\mathbf{x}}_e$ we denote the respective velocities. Then

$$\mathbf{x}_{st} = a \cdot \begin{bmatrix} \sin(\theta_{st}) \\ \cos(\theta_{st}) \end{bmatrix}, \qquad \dot{\mathbf{x}}_{st} = a\dot{\theta}_{st} \cdot \begin{bmatrix} \cos(\theta_{st}) \\ -\sin(\theta_{st}) \end{bmatrix},$$

$$\mathbf{x}_h = l \cdot \begin{bmatrix} \sin(\theta_{st}) \\ \cos(\theta_{st}) \end{bmatrix}, \qquad \dot{\mathbf{x}}_h = l\dot{\theta}_{st} \cdot \begin{bmatrix} \cos(\theta_{st}) \\ -\sin(\theta_{st}) \end{bmatrix},$$

$$\mathbf{x}_{sw} = \mathbf{x}_h + b \cdot \begin{bmatrix} -\sin(\theta_{sw}) \\ -\cos(\theta_{sw}) \end{bmatrix}, \qquad \dot{\mathbf{x}}_{sw} = \dot{\mathbf{x}}_h + b\dot{\theta}_{sw} \cdot \begin{bmatrix} -\cos(\theta_{sw}) \\ \sin(\theta_{sw}) \end{bmatrix},$$

and

$$\mathbf{x}_e = \mathbf{x}_h + l \cdot \begin{bmatrix} -\sin(\theta_{sw}) \\ -\cos(\theta_{sw}) \end{bmatrix}, \qquad \dot{\mathbf{x}}_e = \dot{\mathbf{x}}_h + l\dot{\theta}_{sw} \cdot \begin{bmatrix} -\cos(\theta_{sw}) \\ \sin(\theta_{sw}) \end{bmatrix}.$$

In addition, the line representing the ground is in this coordinate system given by the equation

$$y = -\tan(\gamma) \cdot x.$$

Hence, the requirement of the hip and the swing leg's endpoint to stay above the ground that we mentioned at the beginning of this section can be represented by the conditions

$$\cos(\theta_{st}) \geq -\tan(\gamma) \cdot \sin(\theta_{st}),$$

$$\cos(\theta_{st}) - \cos(\theta_{sw}) \geq -\tan(\gamma) \cdot (\sin(\theta_{st}) - \sin(\theta_{sw})). \tag{4.1}$$

These conditions can be further simplified into

$$-\frac{\pi}{2} + \gamma \leq \theta_{st} \leq \frac{\pi}{2} + \gamma \tag{4.2}$$

and

$$\begin{cases} \theta_{st} + \theta_{sw} \geq 2\gamma \quad \text{and} \quad \theta_{st} - \theta_{sw} \leq 0 & \text{for } \theta_{sw} \geq \gamma \\ \theta_{st} + \theta_{sw} \leq 2\gamma \quad \text{and} \quad \theta_{st} - \theta_{sw} \geq 0 & \text{for } \theta_{sw} < \gamma \end{cases}. \tag{4.3}$$

To derive the dynamics of the system, we will again use Lagrange's method. The kinetic energy T and the potential energy U are given by the sums of kinetic and potential energies at each point mass. Hence, we have

$$T = T_{st} + T_h + T_{sw},$$

$$U = U_{st} + U_h + U_{sw},$$

where

$$T_{st} = \frac{1}{2} m_l \dot{\mathbf{x}}_{st}^T \dot{\mathbf{x}}_{st} = \frac{1}{2} m_l a^2 \dot{\theta}_{st}^2,$$

$$T_h = \frac{1}{2} m_h \dot{\mathbf{x}}_h^T \dot{\mathbf{x}}_h = \frac{1}{2} m_h l^2 \dot{\theta}_{st}^2,$$

$$T_{sw} = \frac{1}{2} m_l \dot{\mathbf{x}}_{sw}^T \dot{\mathbf{x}}_{sw} = \frac{1}{2} m_l \cdot \left(l^2 \dot{\theta}_{st}^2 + b^2 \dot{\theta}_{sw}^2 - 2bl\dot{\theta}_{st}\dot{\theta}_{sw} \cos\left(\theta_{st} - \theta_{sw}\right) \right),$$

and

$$U_{st} = m_l g x_{st2} = m_l g a \cos\left(\theta_{st}\right),$$
$$U_h = m_h g x_{h2} = m_h g l \cos\left(\theta_{st}\right),$$
$$U_{sw} = m_l g x_{sw2} = m_l g \left(l \cos\left(\theta_{st}\right) - b \cos\left(\theta_{sw}\right) \right).$$

The Lagrangian is again given by

$$L = T - U.$$

Since an external torque is present in the model, we must use the more general version of the Euler-Lagrange equations

$$\frac{d}{dt} \left[\frac{\partial L}{\partial \dot{\mathbf{q}}} \right] - \frac{\partial L}{\partial \mathbf{q}} = \frac{\partial W}{\partial \mathbf{q}}, \tag{4.4}$$

where W is the work done by external generalized forces. To compute it for our case of torque τ, first observe that the angle between the two legs is given by $\theta_{st} - \theta_{sw}$. Since τ has counterclockwise direction, the work W can be computed as

$$W = -\tau \left(\theta_{st} - \theta_{sw} \right) = \tau \left(\theta_{sw} - \theta_{st} \right).$$

Because $\mathbf{q}$ consists of two states, we will obtain two equations from (4.4). These are usually written in the form of the so-called *manipulator equations*

$$\mathbf{M}(\mathbf{q})\ddot{\mathbf{q}} + \mathbf{C}(\mathbf{q}, \dot{\mathbf{q}})\dot{\mathbf{q}} = \mathbf{G}(\mathbf{q}) + \mathbf{B}(\mathbf{q})\mathbf{u}. \tag{4.5}$$

Here, $\mathbf{M}(\mathbf{q})$ is the system's inertia matrix, $\mathbf{C}(\mathbf{q}, \dot{\mathbf{q}})$ captures the Coriolis and centrifugal terms, $\mathbf{G}(\mathbf{q})$ the gravity terms, and $\mathbf{B}(\mathbf{q})\mathbf{u}$ the external forces.
For our system, these are given by

$$\mathbf{M}(\mathbf{q}) = \begin{bmatrix} m_l a^2 + m_h l^2 + m_l l^2 & -m_l bl \cos\left(\theta_{st} - \theta_{sw}\right) \\ -m_l bl \cos\left(\theta_{st} - \theta_{sw}\right) & m_l b^2 \end{bmatrix},$$

$$\mathbf{C}(\mathbf{q}, \dot{\mathbf{q}}) = \begin{bmatrix} 0 & -m_l bl \dot{\theta}_{sw} \sin\left(\theta_{st} - \theta_{sw}\right) \\ m_l bl \dot{\theta}_{st} \sin\left(\theta_{st} - \theta_{sw}\right) & 0 \end{bmatrix},$$

$$\mathbf{G}(\mathbf{q}) = \begin{bmatrix} g \sin\left(\theta_{st}\right) \cdot \left(m_l a + m_h l + m_l l \right) \\ -g \sin\left(\theta_{sw}\right) m_l b \end{bmatrix},$$

$$\mathbf{B}(\mathbf{q}) = \begin{bmatrix} -1 \\ 1 \end{bmatrix},$$

and

$$\mathbf{u} = \tau.$$

4.2 Collision Analysis

Now, we will turn our attention to what happens at the moment the swing leg's endpoint hits the ground. This occurs when equality is attained in the condition (4.1). However, due to our assumption that the swing leg retracts when it is in the air, we disregard the possibility of it colliding with the ground when it is behind the stance leg. Putting these two together and using the simplified version (4.3), we obtain that the collision happens when

$$\theta_{st} + \theta_{sw} = 2\gamma \qquad \text{and} \qquad \theta_{st} > \theta_{sw}. \tag{4.6}$$

It follows from our assumption that the legs' collisions are perfectly inelastic and impulsive that the procedure to calculate the biped's state right after a collision as a function of the state right before the collision is just like in the case of the rimless wheel based on the conservation of angular momentum.

We will denote the state right before the collision by

$$\begin{bmatrix} \mathbf{q}(t^-) \\ \dot{\mathbf{q}}(t^-) \end{bmatrix} = \begin{bmatrix} \theta_{st}(t^-) \\ \theta_{sw}(t^-) \\ \dot{\theta}_{st}(t^-) \\ \dot{\theta}_{sw}(t^-) \end{bmatrix}.$$

Similarly, we denote the state right after the collision by

$$\begin{bmatrix} \mathbf{q}(t^+) \\ \dot{\mathbf{q}}(t^+) \end{bmatrix} = \begin{bmatrix} \theta_{st}(t^+) \\ \theta_{sw}(t^+) \\ \dot{\theta}_{st}(t^+) \\ \dot{\theta}_{sw}(t^+) \end{bmatrix}.$$

The relationship between $\mathbf{q}(t^-)$ and $\mathbf{q}(t^+)$ is very simple. The pre-impact stance leg becomes the new swing leg, and the pre-impact swing leg becomes the new stance leg. Essentially, all that occurs there is just relabelling. This can be written as

$$\mathbf{q}(t^+) = \mathbf{R} \cdot \mathbf{q}(t^-), \tag{4.7}$$

where

$$\mathbf{R} = \begin{bmatrix} 0 & 1 \\ 1 & 0 \end{bmatrix} \tag{4.8}$$

and $\mathbf{R}$ stands for *relabel*.

To derive the formula for the new velocities $\dot{\mathbf{q}}(t^+)$, we will need two equations. The first one is the same as in the case of the rimless wheel - the angular momentum of the whole mechanism around the point of collision is preserved. The second one comes from the preservation of angular momentum for the pre-impact stance leg around the robot's hip (see [15]).
We begin with the equation of conservation of angular momentum around the point of

collision with the ground. We first move the coordinate system's origin to $\mathbf{x}_{col}$ as depicted in Fig. 16. We also change the notation of the positions of the pre-impact stance leg and swing leg point masses by $\mathbf{x}_1$ and $\mathbf{x}_2$ to avoid confusion in regards to the relabelling of the legs.

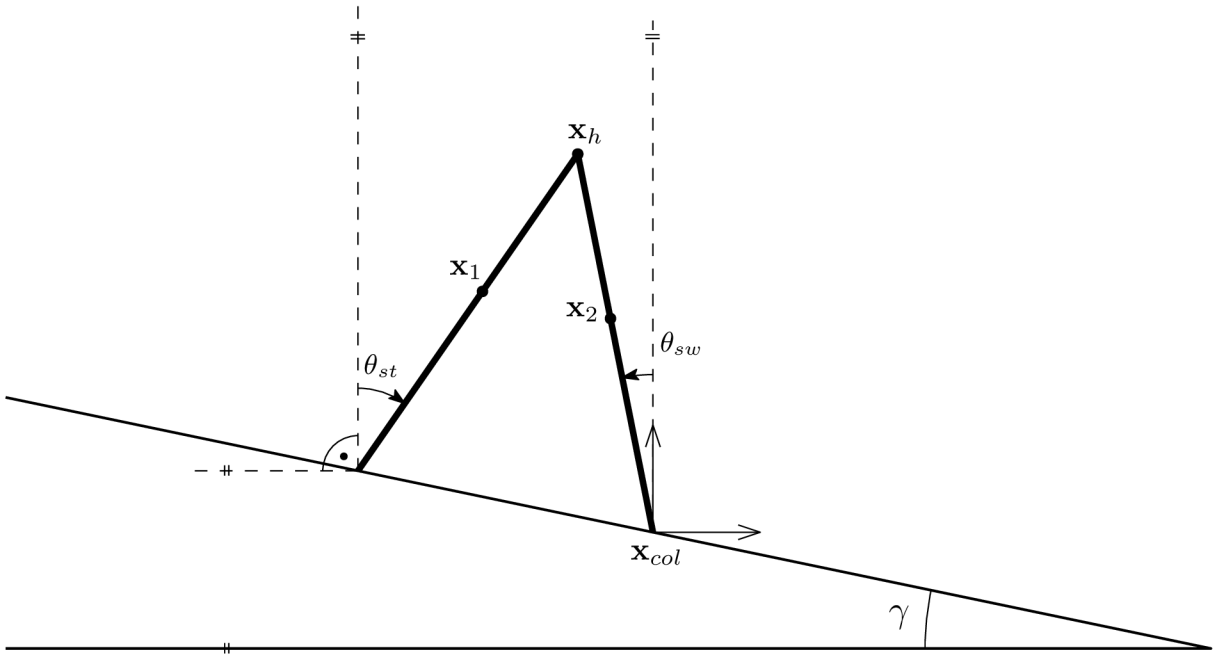

Figure 16. The compass gait biped just before the collision with the coordinate system's origin moved to the point of impact.

The vectors $\mathbf{x}_2$, $\mathbf{x}_h$, and $\mathbf{x}_1$ are in this new coordinate system given by

$$\mathbf{x}_2 = a \cdot \begin{bmatrix} \sin\left(\theta_{sw}(t^-)\right) \\ \cos\left(\theta_{sw}(t^-)\right) \end{bmatrix},$$

$$\mathbf{x}_h = l \cdot \begin{bmatrix} \sin\left(\theta_{sw}(t^-)\right) \\ \cos\left(\theta_{sw}(t^-)\right) \end{bmatrix},$$

$$\mathbf{x}_1 = \mathbf{x}_h + b \cdot \begin{bmatrix} -\sin\left(\theta_{st}(t^-)\right) \\ -\cos\left(\theta_{st}(t^-)\right) \end{bmatrix} = \begin{bmatrix} l\sin\left(\theta_{sw}(t^-)\right) - b\sin\left(\theta_{st}(t^-)\right) \\ l\cos\left(\theta_{sw}(t^-)\right) - b\cos\left(\theta_{st}(t^-)\right) \end{bmatrix}.$$

The positions of the point masses stay the same after the impact, but naturally, their velocities undergo a discontinuous change. We denote the velocities of $\mathbf{x}_1$, $\mathbf{x}_h$, $\mathbf{x}_2$ before and after impact by $\mathbf{v}_1(t^-)$, $\mathbf{v}_h(t^-)$, $\mathbf{v}_2(t^-)$, $\mathbf{v}_1(t^+)$, $\mathbf{v}_h(t^+)$, and $\mathbf{v}_2(t^+)$, respectively. Unlike the positions, they are independent of the origin of the coordinate system. We find them by moving the origin to the end of the stance leg (both for the pre-impact and post-impact state) and differentiating the positions of the point masses with respect to time. It follows that

$$\mathbf{v}_1(t^-) = a\dot{\theta}_{st}(t^-) \cdot \begin{bmatrix} \cos\left(\theta_{st}(t^-)\right) \\ -\sin\left(\theta_{st}(t^-)\right) \end{bmatrix},$$

$$\mathbf{v}_h(t^-) = l\dot{\theta}_{st}(t^-) \cdot \begin{bmatrix} \cos\left(\theta_{st}(t^-)\right) \\ -\sin\left(\theta_{st}(t^-)\right) \end{bmatrix},$$

$$\mathbf{v}_2(t^-) = l\dot{\theta}_{st}(t^-) \cdot \begin{bmatrix} \cos\left(\theta_{st}(t^-)\right) \\ -\sin\left(\theta_{st}(t^-)\right) \end{bmatrix} + b\dot{\theta}_{sw}(t^-) \cdot \begin{bmatrix} -\cos\left(\theta_{sw}(t^-)\right) \\ \sin\left(\theta_{sw}(t^-)\right) \end{bmatrix},$$

$$\mathbf{v}_1(t^+) = l\dot{\theta}_{st}(t^+) \cdot \begin{bmatrix} \cos\left(\theta_{st}(t^+)\right) \\ -\sin\left(\theta_{st}(t^+)\right) \end{bmatrix} + b\dot{\theta}_{sw}(t^+) \cdot \begin{bmatrix} -\cos\left(\theta_{sw}(t^+)\right) \\ \sin\left(\theta_{sw}(t^+)\right) \end{bmatrix},$$

$$\mathbf{v}_h(t^+) = l\dot{\theta}_{st}(t^+) \cdot \begin{bmatrix} \cos\left(\theta_{st}(t^+)\right) \\ -\sin\left(\theta_{st}(t^+)\right) \end{bmatrix},$$

$$\mathbf{v}_2(t^+) = a\dot{\theta}_{st}(t^+) \cdot \begin{bmatrix} \cos\left(\theta_{st}(t^+)\right) \\ -\sin\left(\theta_{st}(t^+)\right) \end{bmatrix},$$

We denote the angular momenta right around to the point of collision before and after the impact by $\mathbf{L}^{(col)}(t^-)$ and $\mathbf{L}^{(col)}(t^+)$. We then have

$$\mathbf{L}^{(col)}(t^-) = \mathbf{x}_1 \times m_l \cdot \mathbf{v}_1(t^-) + \mathbf{x}_h \times m_h \cdot \mathbf{v}_h(t^-) + \mathbf{x}_2 \times m_l \cdot \mathbf{v}_2(t^-), \tag{4.9}$$

$$\mathbf{L}^{(col)}(t^+) = \mathbf{x}_1 \times m_l \cdot \mathbf{v}_1(t^+) + \mathbf{x}_h \times m_h \cdot \mathbf{v}_h(t^+) + \mathbf{x}_2 \times m_l \cdot \mathbf{v}_2(t^+), \tag{4.10}$$

and of course

$$\mathbf{L}^{(col)}(t^-) = \mathbf{L}^{(col)}(t^+). \tag{4.11}$$

This is the first equation for the two unknowns $\dot{\theta}_{st}(t^+)$ and $\dot{\theta}_{sw}(t^+)$. We obtain the second equation by making use of the conservation of momentum for the pre-impact stance leg around the hip. We move the origin of the coordinate system to the robot's hip (as depicted in Fig. 17) and then compute the new position of $\mathbf{x}_1^{(h)}$ (the superscript (h) is there to emphasize the different coordinate system).

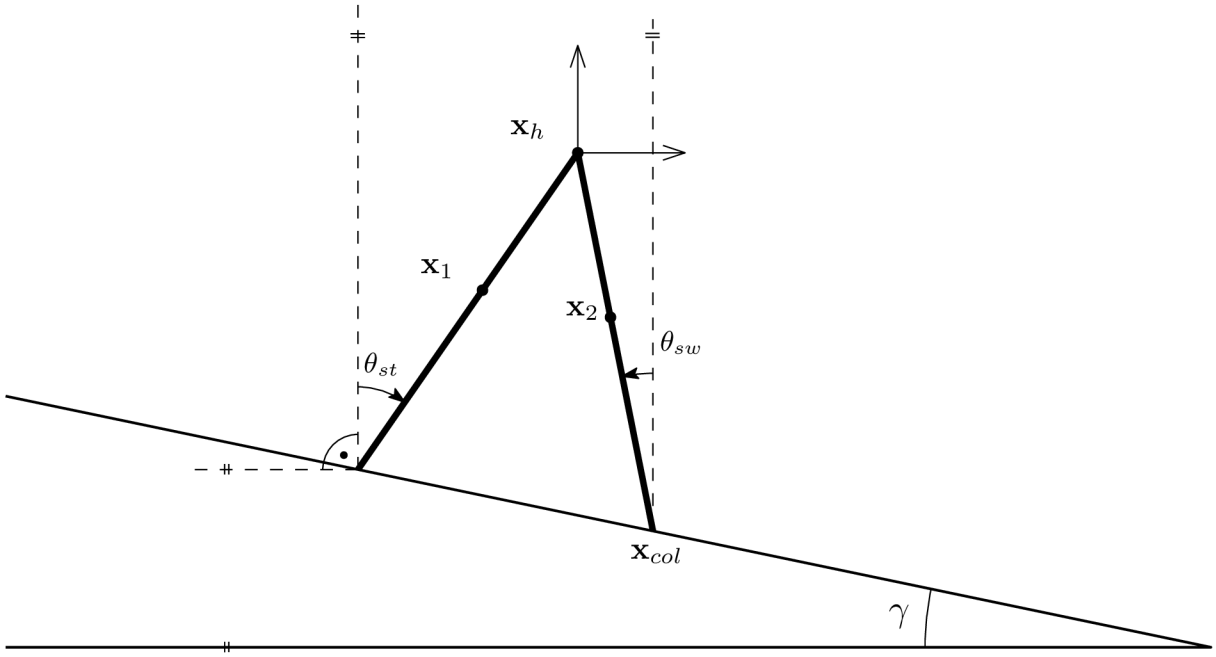

Figure 17. The compass gait biped just before the collision with the coordinate system's origin moved to the biped's hip.

It is simple to verify that

$$\mathbf{x}_1^{(h)} = b \cdot \begin{bmatrix} -\sin\left(\theta_{st}(t^-)\right) \\ -\cos\left(\theta_{st}(t^-)\right) \end{bmatrix}.$$

As we said, the velocities are independent of the origin and so we do not have to calculate them again. We denote the angular momenta of the pre-impact stance leg around the hip right before and after impact by $\mathbf{L}^{(h)}(t^-)$ and $\mathbf{L}^{(h)}(t^+)$, with

$$\mathbf{L}^{(h)}(t^-) = \mathbf{x}_1^{(h)} \times m_l \cdot \mathbf{v}_1(t^-), \tag{4.12}$$

$$\mathbf{L}^{(h)}(t^+) = \mathbf{x}_1^{(h)} \times m_l \cdot \mathbf{v}_1(t^+). \tag{4.13}$$

By setting the momenta equal, we get the second equation.

$$\mathbf{L}^{(h)}(t^-) = \mathbf{L}^{(h)}(t^+). \tag{4.14}$$

As both the equations (4.11) and (4.14) are linear in $\dot{\theta}_{st}(t^+)$ and $\dot{\theta}_{sw}(t^+)$, we can write them in matrix form. By substituting all of the positions and velocities into these equations, we arrive at a system of linear equations

$$\mathbf{Q}_+ \dot{\mathbf{q}}(t^+) = \mathbf{Q}_- \dot{\mathbf{q}}(t^-),$$

where

$$\mathbf{Q}_+ = \begin{bmatrix} m_l\left(-l^2 - a^2 + bl\cos\left(2\alpha\right)\right) - m_h l^2 & m_l\left(-b^2 + bl\cos\left(2\alpha\right)\right) \\ m_l bl\cos\left(2\alpha\right) & -m_l b^2 \end{bmatrix}, \tag{4.15}$$

$$\mathbf{Q}_- = \begin{bmatrix} m_l\left(ab - 2al\cos\left(2\alpha\right)\right) - m_h l^2\cos\left(2\alpha\right) & m_l ab \\ m_l ab & 0 \end{bmatrix}, \tag{4.16}$$

and

$$\alpha = \frac{1}{2}\cdot\left(\theta_{st}(t^-) - \theta_{sw}(t^-)\right).$$

This means that the post-impact vector of velocities is given by the formula

$$\dot{\mathbf{q}}(t^+) = \left(\mathbf{Q}_+^{-1}\mathbf{Q}_-\right)\dot{\mathbf{q}}(t^-). \tag{4.17}$$

Remark. One might wonder why we chose α in this way. The reason is that this, again, nicely connects to the rimless wheel model, where 2α was the angle between two successive legs. In fact, by choosing $\alpha = \frac{1}{2}\cdot\left(\theta_{st}(t^-) - \theta_{sw}(t^-)\right)$, this relation holds for the biped, too. If we substitute $m_l = 0$ into the matrices $\mathbf{Q}_+$ and $\mathbf{Q}_-$, we obtain exactly the equation (3.11). This makes sense because in the rimless wheel case we assumed the weight of the legs to be zero.

At this point, we have all that we need in order to numerically simulate the system. Given initial conditions $\theta_{st}(0)$, $\theta_{sw}(0)$, $\dot{\theta}_{st}(0)$ and $\dot{\theta}_{sw}(0)$, we solve the system of differential equations (4.5), and if the collision condition (4.6) is satisfied, we apply the impact mapping (4.17), thus obtaining a new set of initial conditions. By repeating this procedure ad infinitum, we can compute the state of the system at each time t.

4.3 Numerical Simulation of the Compass Gait Biped

In the previous two sections we derived the swing phase model and the impact model of the biped. We now implement a time simulation of the system in the Python programming language.
To handle the data we use the library NumPy which adds support for n-dimensional matrices and usual linear algebra routines such as multiplying or inverting matrices. In order to integrate the system of differential equations governing the swing phase, we utilize the library SciPy, particularly its function `scipy.integrate.solve_ivp`. The function uses a Runge-Kutta method of the fourth order to solve a given initial value problem. For more information regarding the libraries, see [16] and [17].

To numerically simulate the system, we need to turn the system of differential equations (4.5), the collision condition (4.6), and the collision transition (4.17) into code.
We then define a function that takes in initial conditions and a final time `T` as arguments. It first solves the initial value problem for time in the interval $(0, \mathtt{T})$, then it runs a collision detection procedure which returns the time of collision $\mathtt{T}^*$. The function then cuts off the solution on the rest of the interval, applies the impact transition function and updates its initial conditions accordingly. The same procedure is repeated until all of time `T` is used up. At this point, the function returns a list of all the individual swing phase trajectories. The code is available in Appendix A.

4.4 The Poincaré Map

Just like before, we introduce a return map for the system in order to convert the problem of finding a limit cycle (representing the biped walking) to the language of discrete dynamical systems. We use the same notation as in Subsection 3.3.1. However, this time we cannot simplify the analysis and only care about the angular velocity at the beginning of each step. Instead, we will define the map for the system's entire state.
By

$$\mathbf{\Phi}_n = \begin{bmatrix} \mathbf{q}_n \\ \dot{\mathbf{q}}_n \end{bmatrix},$$

we denote the system's state right after its swing leg impacts the ground. This in itself defines the return map. However, unlike in the rimless wheel case, we do not have a formula for $\mathbf{q}(t^-)$ for given initial data $\mathbf{q}(0)$. If by $\mathbf{\Phi}_n^-$ we denote the state of the system just before an impact, with initial conditions $\mathbf{q}(0) = \mathbf{q}_n$, $\dot{\mathbf{q}}(0) = \dot{\mathbf{q}}_n$, then a recursive definition for the Poincaré map similar to (3.13) and (3.14) can be written in a block matrix form as

$$\mathbf{\Phi}_{n+1} = \left[\begin{array}{c|c} \mathbf{R} & \mathbf{O} \\ \hline \mathbf{O} & \mathbf{Q}_+^{-1}\mathbf{Q}_- \end{array}\right] \cdot \mathbf{\Phi}_n^-. \tag{4.18}$$

In this definition, the matrices $\mathbf{R}$, $\mathbf{Q}_-$, and $\mathbf{Q}_+$ are taken as defined in formulas (4.8), (4.15), and (4.16), respectively. The symbol $\mathbf{O}$ on the other hand represents a 2×2 matrix of zeros.

4.4.1 Fixed Points of the Poincaré Map

A natural question that immediately follows is if the map introduced in (4.18) has fixed points. These points would correspond to periodic solutions of the system, which in turn carry the meaning of the biped walking down the slope. Even more intriguing is the problem of existence of fixed points for *passive walking*, i.e. with $\tau = 0$, simplifying the equation (4.5) governing the swing dynamics to

$$\mathbf{M}(\mathbf{q})\ddot{\mathbf{q}} + \mathbf{C}(\mathbf{q}, \dot{\mathbf{q}})\dot{\mathbf{q}} = \mathbf{G}(\mathbf{q}). \tag{4.19}$$

This would indicate that this system which is much more complicated than the simple rimless wheel studied in Section 3 would also be able to exhibit a neverending rolling-like behavior.

Indeed, it has been shown (see [2]) that these fixed points can exist, at least for small slopes γ. Our goal is to implement a numerical method to search for them.

4.4.2 Numerical Search for Fixed Points of the Poincaré Map

To begin, we define the problem that we want to solve.

Problem 4.1. Find an element from the state space $\mathbf{\Phi}_1$ so that it is a fixed point of the Poincaré map.

Before we introduce the numerical algorithm that solves Problem 4.1, we first reformulate it into an equivalent problem that is easier to handle. First, observe that if $\mathbf{\Phi}_1$ is a fixed point, then by definition

$$\mathbf{\Phi}_2 = \mathbf{\Phi}_1.$$

Because given a $\mathbf{\Phi}_1$ we can find $\mathbf{\Phi}_2$ numerically, if we introduce a metric d on the state space, the problem can then be thought of as the problem of minimizing $d(\mathbf{\Phi}_1, \mathbf{\Phi}_2)$. This is justified because any metric is non-negative and attains 0 if and only if the two elements are equal. Since the state space is a subset of $\mathbb{R}^4$, we can use the usual Euclidean metric.

Next, consider that for $\mathbf{\Phi}_1$ to be a fixed point of the Poincaré map, it must necessarily lie on the impact surface defined by (4.6), only with θ_{st} and θ_{sw} swapped because $\mathbf{\Phi}_1$ represents the state right *after* a collision (refer to (4.7)). This allows us to reduce the dimension of the set of admissible states among which we are looking for the "best" one.

However, we do not even have to search exactly for states that lie on the impact surface. Any state that belongs to the trajectory that starts with initial conditions that lead to a perodic solution solves the problem. From the nature of the system, we know that this periodic solution must pass through the hyperplane

$$\theta_{st} = \theta_{sw}. \tag{4.20}$$

This is so because at the beginning of the step the state angles satisfy $\theta_{st} < \theta_{sw}$, and at the end we have $\theta_{st} > \theta_{sw}$ instead. Because the functions $\theta_{st}(t)$ and $\theta_{sw}(t)$ are continuous in the swing phase, there must exist a time t^* when $\theta_{st}(t^*) = \theta_{sw}(t^*)$.

This reasoning leads us to redefining Problem 4.1 as follows.

Problem 4.2. Find initial conditions $(\theta_{st}(0), \theta_{sw}(0), \dot{\theta}_{st}(0), \dot{\theta}_{sw}(0))$ satisfying $\theta_{st}(0) = \theta_{sw}(0)$ such that $d(\mathbf{\Phi}_1, \mathbf{\Phi}_2)$ is minimized, where

$$d(\mathbf{\Phi}_1, \mathbf{\Phi}_2) = \sum_{i=1}^{4} \left(\mathbf{\Phi}_{2i} - \mathbf{\Phi}_{1i}\right)^2$$

.

The choice of sampling the trajectory at $\theta_{st} = \theta_{sw}$ has the added benefit that we can at least have a rough estimate of the position of the initial conditions in the state space. Namely, one can expect that $\theta_{st}(0)$ is very close to 0, $\dot{\theta}_{st}(0)$ is positive, and that $\dot{\theta}_{sw}(0)$ is negative. These assumptions are of substantial help when it comes to the time complexity of any potential algorithm.

We implement the minimization algorithm in Python, using the solver described in Subsection 4.3. To begin, we must define the feasible region Ω_F and the objective function. The set of feasible solutions $\left(\theta_{st}, \dot{\theta}_{st}, \dot{\theta}_{sw}\right)$ is a subset of $\mathbb{R}^3$ satisfying the assumptions outlined in the paragraph above. For small slopes of $\gamma < 0.06$, we found

$$\Omega_F = (-0.2, 0.2) \times (0, 1) \times (-3, 0)$$

to be a good starting point.
The objective function should return a positive value to each element of the feasible region. If $(x_1, x_2, x_3) \in \Omega_F$, then the function first creates an initial condition $\theta_{st}(0) = x_1, \theta_{sw}(0) = x_1, \dot{\theta}_{st}(0) = x_2, \dot{\theta}_{sw}(0) = x_3$ according to (4.20), and then runs the solver described earlier. If the solution does not successfully complete at least two cycles, it is discarded. On the other hand, if it does, the objective function returns the value $d(\mathbf{\Phi}_1, \mathbf{\Phi}_2)$ defined in Problem 4.2.

The function that minimizes the objective function on Ω_F is divided into two phases. First, it runs a simple brute-force grid search over Ω_F to find a very rough first estimate. In the second phase, we increase the time-step density for our solver to decrease the error caused by inaccurate collision detections, run it, and collect the last $\mathbf{\Phi}_n$ in the sequence. The code is available in Appendix B.

An example of the result for a particular set of parameters is given in Fig. 18. Visualizing the solution is inherently trickier than in the case of the rimless wheel because of the higher dimension of the problem. However, for periodic solutions, one leg's trajectory is the same as the other one's is in the next cycle. Fig. 18 shows one full cycle, the top part being the trajectory of the stance leg, and the bottom part that of the swing leg. The collision transition is indicated by the dashed lines.

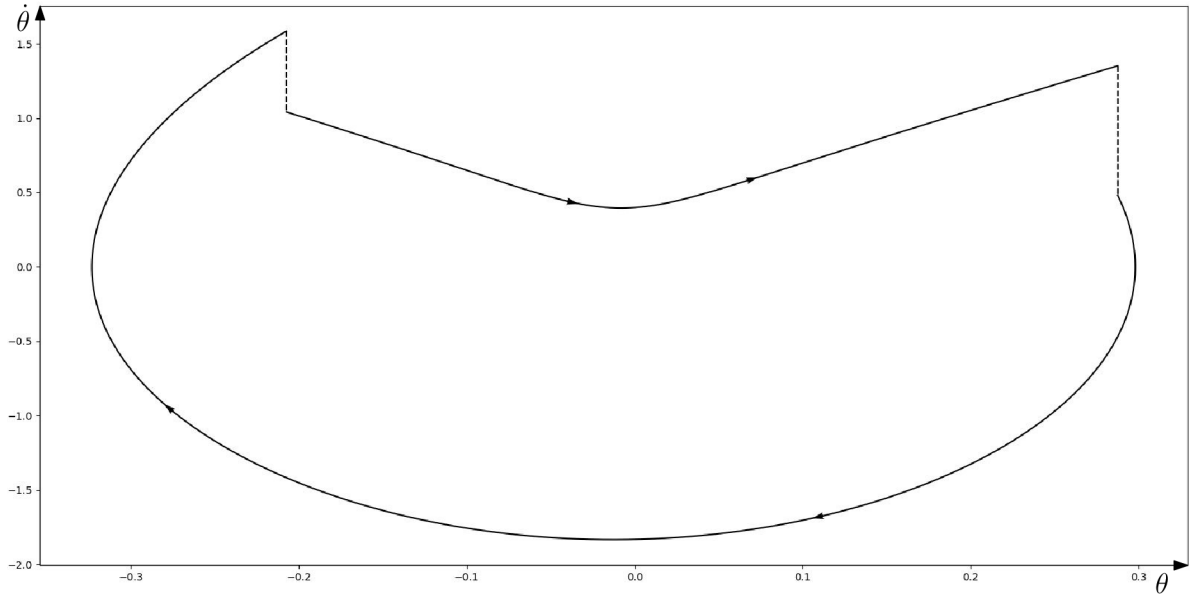

Figure 18. A periodic solution of the system found for the parameters $m_h = 10, \quad m_l = 5, \quad a = 0.5, \quad b = 0.5, \quad g = 9.81, \quad \gamma = 0.04$ and initial conditions $\theta_{st}(0) = -0.207, \quad \theta_{sw}(0) = 0.287, \quad \dot{\theta}_{st}(0) = 1.041, \quad \dot{\theta}_{sw}(0) = 0.481)$.

5 Conclusions

This thesis dealt with mathematical models of walking robots. In particular, the rimless wheel model and the compass gait biped model were chosen for study. The thesis is divided into three main chapters.
In the first chapter, some of the necessary mathematical apparatus was introduced. This includes the theory of dynamical systems. The differences between continuous, discrete, and hybrid systems were explained. Some definitions connected to the notion of stability were also stated. The link between continuous and discrete systems in the form of the Poincaré map was explained. A brief mention of Euler-Langrange equations was included as well.

The topic of the second chapter was the rimless wheel model. A short description of the model was followed up by a derivation of the differential equation governing its swing phase (see (3.2)). Formulas for the angular velocity at the end of the step with respect to the initial angular velocity were derived for the forward, the backward, and the rocking regimes of the wheel (see (3.5), (3.8), and (3.10), respectively). The impact model based on the law of conservation of angular momentum was derived in Subsection 3.2. The loss of energy due to dissipation was also obtained in (3.12).
Next, the long-term behavior of the wheel was examined. The analysis was approached via the introduction of a Poincaré map, thus transforming the question of stability of possible periodic cycles of the hybrid system into a discussion of stability of the map's fixed points. Some of the map's properties used in later theorems were stated and proved in Section 3.3.2. The conditions for the map's fixed points' existence were derived. It was shown that the map has only two possible fixed points, ω^*_{stop} (corresponding to the wheel's motion stopping) and ω^*_{roll} (corresponding to the wheel's moving downwards at constant speed). Formulas for the values of fixed points based on the parameters specifying the model were also presented.
Then, theorems regarding the conditions for stability of these fixed points were stated and proved. It was shown that the region $\Omega_{(\alpha,\gamma)}$ of admissible angles α and γ can be divided into five disjunctive subregions for which the long-term behavior of the wheel differs. Precise formulas for the regions of attraction of both fixed points for each subregion of $\Omega_{(\alpha,\gamma)}$ were found.
The results of the second chapter were summarized in Subsection 3.4. A table (see Table 1) discussing the properties of the fixed points and their regions of attraction for each of the subregions of $\Omega_{(\alpha,\gamma)}$ was included, as well as a visualization of $\Omega_{(\alpha,\gamma)}$ in Fig. 14.

The third chapter deals with the compass gait model. The model and its assumptions were described and explained. The system of differential equations controlling its swing phase was derived and written in the form of the manipulator equations (4.5).
The collision conditions were found and stated in (4.3). The impact model based on the two instances of conservation of angular momenta was derived. The momentum must be conserved for the whole mechanism around the point where the swing leg collides with the ground, and also for the stance leg around the biped's hip. The impact model was summarized in formulas (4.8) and (4.17).
Analogically to the rimless wheel, a Poincaré map was defined for the biped. A solver for the model was implemented in Python. Finally, a method for finding fixed points of the Poincaré map corresponding to the biped's walking down the ramp was also implemented.

The Python files were included in the appendix.

The main goals of the thesis were achieved. The hybrid dynamical systems underlying the two chosen models were derived, together with ample explanations of the techniques used. Most of the work was done on the rimless wheel model, where a comprehensive analysis was carried out. The model's long term behavior is essentially "solved" in the thesis. For the other model, the tools used for the rimless wheel were transformed into numerical methods. However, here, more work could have been done in regard to the control of the biped via the actuator placed in its hip. In this aspect, the thesis is incomplete. Nevertheless, it turns out that the control of the presented bipedal robot involves many aspects that have to be taken into consideration.

There are many possible directions by which the thesis can be followed up on. After all, the two chosen models are only a tiny part of the growing field of robotic walking. For instance, the compass gait biped model can be improved by adding knee joints to each of the legs. This idea is demonstrated for example in [18].
Another possibility is the use of control theory techniques to enlarge the stability region of the biped's passive gait. An example of this approach is described in [19].

References

[1] KAJITA, S., ESPIAU, B., 2008. *Legged Robots. Springer Handbook of Robotics.* Pages 361–389.

[2] MCGEER, T., 1990. *Passive dynamic walking.* International Journal of Robotics Research. Pages 62-82.

[3] BOSTON DYNAMICS. *More Parkour Atlas* [online]. Youtube, September 2019. [cit. 26. 6. 2020]. Available at: <https://www.youtube.com/watch?v=_sBBaNYex3E>.

[4] BOSTON DYNAMICS. *What's new, Atlas?* [online]. Youtube, November 2017. [cit. 26. 6. 2020]. Available at: <https://www.youtube.com/watch?v=fRj34o4hN4I>.

[5] TEDRAKE, R., 2020. *Underactuated Robotics: Algorithms for Walking, Running, Swimming, Flying, and Manipulation* [online]. [cit. 12. 6. 2020]. Available at: <http://underactuated.mit.edu/>.

[6] STROGATZ, S., 2015. *Nonlinear Dynamics and Chaos: with Applications to Physics, Biology, Chemistry, and Engineering.* Boulder, CO: Westview Press, a member of the Perseus Books Group.

[7] MODELICA. *Bouncing Ball* [online]. Modelica. [cit. 26. 6. 2020]. Available at: <https://mbe.modelica.university/behavior/discrete/bouncing/>.

[8] VERHULST, F., 1990. *Nonlinear differential equations and dynamical systems.* Springer-Verlag, Berlin, Heidelberg.

[9] PERKO, L., 2001. *Differential equations and dynamical systems.* Springer. New York.

[10] MORRIS, B., GRIZZLE, J., 2005. *A restricted Poincaré map for determining exponentially stable periodic orbits in systems with impulse effects: Application to bipedal robots.* Proceedings IEEE 44th Annual Conference on Decision and Control (CDC), 4199–4206.

[11] MORIN, D., 2008. *Introduction to classical mechanics: with problems and solutions.* Cambridge University Press.

[12] LAGRANGE, J., 2009. *Mécanique Analytique (Cambridge Library Collection - Mathematics).* Cambridge University Press.

[13] ARNOLD, V.I., 1989. *Mathematical Methods of Classical Mechanics.* 2. New York: Springer Verlag. ISBN 978-0-387-96890-2.

[14] JUCHEM NETO, J. P., 2017. *Solving the nonlinear pendulum equation with nonhomogeneous initial conditions.* International Journal of Applied Mathematics.

[15] GARCIA, M., CHATTERJEE, A., RUINA, A., COLEMAN, M., 1998. *The simplest walking model: Stability, complexity, and scaling.* Journal of biomechanical engineering. 120. 281-8.

[16] NUMPY. *NumPy Reference* [online]. NumPy. [cit. 26. 6. 2020]. Available at: <https://numpy.org/doc/stable/reference/index.html>.

[17] SCIPY. *SciPy Reference* [online]. SciPy. [cit. 26. 6. 2020]. Available at: <https://docs.scipy.org/doc/scipy/reference/>.

[18] ZHANG, P., TIAN, Y., LIU, Z., YANG, S., TIAN, R., 2008. *Further Research and Comparison of Gaits for Compass-Like Biped and Kneed Passive Dynamic Walker.* Intelligent Robotics and Applications. Lecture Notes in Computer Science, vol 5314. Springer, Berlin, Heidelberg.

[19] SPONG, M., 1999. *Passivity based control of the compass gait biped.* IFAC Proceedings Volumes, Volume 32, Issue 2. Pages 506-510.

Appendix A: The Compass Gait Biped Solver

```
import math
import numpy as np
from scipy import integrate

'''The parameters specifying the compass gait model'''
gamma = 0.04
g = 9.81
a = 0.5
b = 0.5
l = a + b
m_h = 10
m_l = 5
tau = 0

'''The system of differential equations governing the swing phase model.
   As an input, it takes the time and current state of the system. It returns the right-hand side of
   the equation x_dot = f(x).'''

def diffeq(t, state):
    x_1 = state[0]
    x_2 = state[1]
    x_3 = state[2]
    x_4 = state[3]

    #The matrices M, C, G, and B defined in Subsection 4.1
    M = np.matrix([[m_l*a*a + m_h*l*l + m_l*l*l, -m_l*b*l*math.cos(x_1 - x_2)], [-m_l*b*l*math.cos(x_1 - x_2), m_l*b*b]])
    C = np.matrix([[0, -m_l*b*l*x_4*math.sin(x_1 - x_2)], [m_l*b*l*x_3*math.sin(x_1 - x_2), 0]])
    G = np.matrix([[g*math.sin(x_1)*(m_l*a + m_h*l + m_l*l)], [-g*math.sin(x_2)*m_l*b]])
    B = np.matrix([[-1], [1]])
    u = tau
    acc = np.linalg.inv(M)*(-C*np.matrix([[x_3], [x_4]]) + G + B*u)

    return [x_3, x_4, float(acc[0]), float(acc[1])]


'''The function that detects the time of collision based on an input of arrays of theta_st and theta_sw
   according to the collision conditions (4.2) and (4.3).'''

def detect_collision(arr_1, arr_2):
    for i in range(len(arr_1)):
        if arr_1[i] + arr_2[i] > 2*gamma and arr_1[i] > arr_2[i]:
            return [i, 'leg']
        if arr_1[i] > math.pi/2 + gamma or arr_1[i] < -math.pi/2 + gamma:
            return [i, 'hip']

    return [len(arr_1) - 1, 'nothing']


'''The solver of the compass gait biped model. It takes an initial condition, a final time, and density of
   the time interval as inputs. By density, we mean the number of interpolation points
   in the interval [0, T].
   It returns the collection of individual swing phase trajectories.'''

def simul(state, T, density):
    state = state
    bad = False

    trajectories = []
    totaltime = T
    time_subtracted = 0

    while (totaltime > 0):
```

```
62          timerange = [0, totaltime]
63          t = np.linspace(0, totaltime, density)
64          traj = integrate.solve_ivp(diffeq, timerange, state, dense_output=True)
65          traj = traj.sol(t)
66
67          [index, collision] = detect_collision(traj[0], traj[1])
68             #If a collision of the hip with the ground or an extremely short swing phase
               time corresponding
69             #to the biped stumbling is detected, the function terminates.
70          if collision is 'hip' or t[index] < 0.05:
71              new_traj = [t[:index] + time_subtracted, traj[0][:index], traj[1][:index],
                traj[2][:index], traj[3][:index]]
72              trajectories.append(new_traj)
73              bad = True
74              return [trajectories, bad]
75
76          if collision is 'nothing':
77              trajectories.append([t + time_subtracted, traj[0], traj[1], traj[2],
                traj[3]])
78              totaltime -= T
79
80             #If a collision of the swing leg with the ground is detected, the remaining
               portion of the time interval
81             #is discarded and a new swing phase starts, with initial conditions
82             #based on the formulas (4.7) and (4.17).
83          else:
84              new_traj = [t[:index] + time_subtracted, traj[0][:index], traj[1][:index],
                traj[2][:index], traj[3][:index]]
85              trajectories.append(new_traj)
86              alpha = 0.5*(traj[0][index] - traj[1][index])
87              Q_1 = np.matrix([[m_l*(-l*l -a*a + b*l*math.cos(2*alpha)) - m_h*l*l,
                m_l*(-b*b +b*l*math.cos(2*alpha))], [m_l*b*l*math.cos(2*alpha), -m_l*b*b]])
88              Q_2 = np.matrix([[m_l*(a*b - 2*a*l*math.cos(2*alpha)) -
                m_h*l*l*math.cos(2*alpha), m_l*a*b], [m_l*a*b, 0]])
89              old_vels = np.matrix([[traj[2][index - 1]], [traj[3][index - 1]]])
90              new_vels = np.linalg.inv(Q_1)*Q_2*old_vels
91              state = [traj[1][index - 1], traj[0][index - 1], float(new_vels[0]),
                float(new_vels[1])]
92              totaltime -= t[index - 1]
93              time_subtracted += t[index - 1]
94      return [trajectories, bad]
95
96  '''Initial conditions [theta_st, theta_sw, dot_theta_st, dot_theta_sw]'''
97  state= [-0.20741034501258232, 0.2874189924188885, 1.0409143102934366, 0.4808181141599959]
98
99  '''The simulation's final time'''
100 T = 10
101
102 '''Density of the time interval'''
103 density = 500000
104
105 [solution, bad] = simul(state, T, density)
106 if bad:
107     print('The hip of the robot has collided with the ground.')
```

Appendix B: Numerical Search for Passive Gaits

```
'''THE COMPASS GAIT BIPED SOLVER simul() IS REQUIRED TO RUN THIS SCRIPT'''



'''The cost function based on the Euclidean metric. For every state it returns a non-negative
   number measuring how close it is to the passive gait state.'''
def cost_function(state, density):
    T = 5
    [solution, bad] = simul(state, T, density)
    #if the solution does not have at least two cycles or its hip collides with the ground,
    #the function returns an artificial penalty
    if len(solution) < 3 or bad:
        cost = 1000
    #otherwise, it returns the euclidean metric between two successive Poincare maps
    else:
        s_1 = solution[1]
        s_2 = solution[2]
        cost = (s_2[1][0]-s_1[1][0])**2 + (s_2[2][0]-s_1[2][0])**2 +
        (s_2[3][0]-s_1[3][0])**2 + (s_2[4][0]-s_1[4][0])**2
    return cost

'''A wrapper for the cost function based on the insights described in Subsection 4.4.2'''
def cost_wrapper(params, density):
    return cost_function([params[0], params[0], params[1], params[2]], density)

'''A basic grid search for a subset of the R^3 space defined by the 'ranges' argument.
   It partitions the subset into n^3 evenly spaced grid points and evaluates the function 'f' at
   each one of them. It returns the lowest value of f and its minimizer.'''
def grid_search(f, ranges, n, density):
    stepsize=[]
    for i in ranges:
        stepsize.append((i[1] - i[0])/(n-1))

    glob_min = 1000
    x_min = [ranges[0][0], ranges[1][0], ranges[2][0]]
    for i in range(n+1):
        for j in range(n+1):
            for k in range(n+1):
                x = [ranges[0][0] + i*stepsize[0], ranges[1][0] + j*stepsize[1],
                ranges[2][0] + k*stepsize[2]]
                val = cost_wrapper(x, density)
                if val < glob_min:
                    glob_min = val
                    x_min = x
    return [x_min, glob_min]

'''The main function. If there exists one, it finds the fixed point of the Poincare map
   in the subset of R^3 specified by the argument 'bounds'. The value 'n' specifies the
   partition of the subset for the initial grid search. The arguments 'initial_density' and 'final_density'
   specify the density of the time interval partition for the compass gait biped solver. '''
def find_passive_gait(bounds, n, initial_density, final_density):
    #phase 1: a grid search in the regions defined by bounds
    [x_0, cost] = grid_search(cost_wrapper, bounds, n, initial_density)

    #phase 2: take the grid search solution as an initial guess and run the solver with a higher
    #time interval density so that it converges to a better solution naturally while minimizing the error
    #caused by an inaccurate collision detection
    T = 10
    [solution, bad] = simul([x_0[0], x_0[0], x_0[1], x_0[2]], T, final_density)
    return [[solution[-1][1][0], solution[-1][2][0], solution[-1][3][0],
```

```
        solution[-1][4][0]], cost]

a_1 = -0.2
b_1 = 0.2
a_2 = 0
b_2 = 1
a_3 = -3
b_3 = 0
n = 8
bounds = ((a_1, b_1), (a_2, b_2), (a_3, b_3))
initial_density = 1000
final_density = 500000

[omega_roll, cost] = find_passive_gait(bounds, n, initial_density, final_density)
print(omega_roll)
print(cost)
```

List of Abbreviations and Symbols

$\mathbb{R}$	the set of real numbers
$\mathbb{N}$	the set of natural numbers (starting with 1)
$\mathbb{Z}$	the set of integers
d	a metric
f^n	an iteration of n compositions of the function f
L	the Lagrangian of a system
T	the kinetic energy of a system
U	the potential energy of a system
W	the work done by generalized external forces
g	gravitational acceleration
l	the length of a leg
m	the mass of the rimless wheel
γ	the angle of the ramp's slope
α	one half of the angle between two legs
θ	the angle of the rimless wheel's stance leg
$\Omega_{(\alpha,\gamma)}$	the region of possible configurations of α and γ for the rimless wheel
$\Omega_1, \Omega_2, \Omega_3, \Omega_4, \Omega_5$	disjunctive partitions of $\Omega_{(\alpha,\gamma)}$
$\mathbf{q}$	the vector of generalized coordinates
ω_f	the critical angular velocity for making a step forward defined in (3.4)
ω_b	the critical angular velocity for making a step backward defined in (3.7)
$\mathbf{L}$	angular momentum
$\dot{\theta}_n$	the angular velocity of the wheel right after the n^{th} collision
H_1, H_2, H	the sets of heteroclinic orbits of the rimless wheel and their union as defined in Definition 3.6

$\omega^*_{stop}, \omega^*_{roll}$	fixed points of the Poincaré map
$R_A(\omega^*_{stop}), R_A(\omega^*_{roll})$	the fixed points' regions of attraction
a	the distance of the compass gait biped's leg mass from the leg's endpoint
b	the distance of the compass gait biped's leg mass from the hip
m_h	the mass of the biped's hip
m_l	the mass of each of the biped's legs
θ_{st}	the angle of the biped's stance leg
θ_{sw}	the angle of the biped's swing leg
$\mathbf{R}$	the relabel matrix defined in (4.8)
$\mathbf{Q}_+, \mathbf{Q}_{+-}$	the impact matrices defined in (4.15) and (4.16)
$\mathbf{\Phi}_n$	the state of the biped right after the n^{th} collision